Monitoreo de la actividad sísmica del territorio colombiano usando aprendizaje profundo

Emmanuel David Castillo Taborda

Universidad Nacional de Colombia
Facultad de Ciencias, Departamento de Geociencias.
Bogotá, Colombia
2022

Estudiante
Emmanuel David Castillo Taborda
CC 1037658661
ecastillot@unal.edu.co

Director de Tesis
Germán Andrés Prieto Gómez
gaprietogo@unal.edu.co

Monitoring seismic activity in the Colombian territory using Deep Learning

Emmanuel David Castillo Taborda

A thesis submitted in fulfillment of the requirements for the degree of:
Magíster en Ciencias: Geofísica

Supervisor:
Ph.D. Germán Andrés Prieto Gómez

Universidad Nacional de Colombia
Facultad de Ciencias.Departamento de Geociencias
Bogotá, Colombia
2022

"Much of what is known about earthquakes follows from study of the motion of the ground"
- Charles Richter, *Elementary Seismology*, 1958

Acknowledgment

I would like to express my deep gratitude to my supervisor, Professor Germán Prieto, for his patient guidance and for selflessly transmitting his knowledge to me. Also, I would like to extent my acknowledgment to Daniel Siervo, seismologist in the Colombian Geological Survey, who contributed seismological and computational knowledge. Also, they give me enthusiastic encouragement and useful critiques for this research work.

I would also like to thank the professionals of the Colombian Seismological Network, specially the analyst, seismology and systems teams, for their disposition to help me with several seismological and technical issues. In general, I also thank the Geological Service for authorizing the processing of seismological data.

Finally, I must thank all my family, girlfriend and friends, who always believed in me and have given me all the support I need to continue.

Abstract

Seismological networks, whether global, regional, or local, have the objective of monitoring seismic activity. This implies the detection of seismic events and determination of their location (latitude, longitude, depth and origin time) with an acceptable level of uncertainty. We apply these steps in three seismic networks automatically. A regional seismic network (Colombian Seismological Network-CM, station separation $\sim$ 100 km), and two local and temporary networks (station separation $\sim$ 10-30 km) in northern South America: the Middle Magdalena Valley Array (VMM), and the Carribean-Mérida Andes seismic array (YU).

To achieve this, continuous data of multiple stations needs to be processed to detect and pick seismic phases (usually body waves). In many networks this process is carried out by an analyst who, visually examining the traces, determines the arrival time of a wave at a station. However, for dense seismic networks or temporary deployments, this task can be very laborious, requiring several analysts. To detect and pick the seismic phases automatically of the CM network, we use two pre-trained Deep Learning models: EQTransformer and PhaseNet. We derive some statistics to compare the performance in both reliability and compatibility with the Scanloc association and location algorithm. Based on the above, we use only EQTransformer for the two local networks.

The CM catalog generated by the PhaseNet and EQTransformer picks was compared with the manual catalog. Both catalogs are sufficiently reliable to show asimilar distribution of intermediate and shallow seismicity in the Colombian territory. The local networks show a more detailed patterns of seismicity locations. At last, we merge the catalogs in only one automatic seismic catalog and use some transects to identify regional tectonic structures and highlight regional faults. The results show that this implementation is reliable enough to generate automatic seismic catalogs with the appropriate quality in terms of the event location errors and is capable of defining major tectonic structures. Better yet, it can improve earthquake processing times and complement manual catalogs due to its good performance for small earthquakes and aftershocks.

Key Words: Deep learning, Autopicking, PhaseNet, EQTransformer, Colombian seismicity.

Resumen

Las redes sismológicas, ya sean mundiales, regionales o locales, tienen como objetivo vigilar la actividad sísmica. Esto implica la detección de eventos sísmicos y la determinación de su localización (latitud, longitud, profundidad y tiempo de origen) con un nivel aceptable de incertidumbre. Aplicamos estos pasos en tres redes sísmicas de forma automática. Una red sísmica regional (Red Sismológica Colombiana-CM, separación entre estaciones $\sim$ 100 km), y dos redes locales y temporales (separación entre estaciones $\sim$ 10-30 km) en el norte de Suramérica: Las redes sísmicas locales del Valle Medio de Magdalena (VMM) y de los Andes del Caribe-Mérida (YU).

Para ello, es necesario procesar los datos continuos de múltiples estaciones para detectar y picar las fases sísmicas (normalmente ondas de cuerpo). En muchas redes, este proceso lo lleva a cabo un analista que, examinando visualmente las trazas, determina el tiempo de llegada de cada onda a una estación. Sin embargo, en redes sísmicas densas o en despliegues temporales, esta tarea puede ser muy laboriosa y requerir varios analistas. Para detectar y picar las fases sísmicas automáticamente de la red CM, utilizamos dos modelos de Deep Learning pre-entrenados: EQTransformer y PhaseNet. Derivamos algunas estadísticas para comparar el rendimiento tanto en fiabilidad como en compatibilidad con el algoritmo de asociación y localización Scanloc. Basándonos en lo anterior, utilizamos solo EQTransformer para las dos redes locales.

El catálogo CM generado por los picks de PhaseNet y EQTransformer se comparó con el catálogo manual. Ambos catálogos son suficientemente confiables para mostrar una distribución similar de la sismicidad intermedia y somera del territorio colombiano. Las redes locales muestran un patrón más detallado de la localización de la sismicidad. Por último, fusionamos los catálogos en uno solo catálogo sísmico automático y usamos algunos cortes para identificar estructuras tectónicas regionales y resaltar fallas regionales. Los resultados muestran que esta implementación es lo suficientemente fiable como para generar catálogos sísmicos automáticos con la calidad adecuada en términos de errores de localización de eventos y es capaz de definir las principales estructuras tectónicas. Mejor aún, puede mejorar los tiempos de procesamiento de terremotos y complementar los catálogos manuales gracias a su buen rendimiento para terremotos pequeños y réplicas.

Palabras claves: Aprendizaje Profundo, Autopicado, PhaseNet, EQTransformer, Sismicidad Colombiana.

List of Figures

Contents

1 Introduction

The amount of seismological data has been increasing both globally [Suárez et al., 2008, Ringler et al., 2019, Londoño et al., 2019], with the growth of seismological networks, continuous monitoring, and the deployment of local or temporary networks for specific studies [Cornthwaite et al., 2017, Londoño et al., 2019, Molina et al., 2020]. This increase has also allowed an increase in the number of detected earthquakes or characterized seismic events and also the identification of seismic activity that previously went unnoticed.

With the increase in data volume has also come the need to develop computational tools that are capable of processing, analyzing and detecting seismic events (due to the volume of data). These developments include automatic earthquake detection methods (STA/LTA) [Allen, 1978, Trnkoczy, 2009, Liu and Zhang, 2014, Kumar et al., 2018], event detection using template matching [Gibbons and Ringdal, 2006, Ross et al., 2019a, Lee et al., 2020], Fingerprint and Similarity Thresholding methods (FAST) [Bergen and Beroza, 2019] and more recently Machine Learning methods to detect events and/or determine the arrival of seismic waves [Ross et al., 2018a, Ross et al., 2018b, Zhu and Beroza, 2019, Woollam et al., 2019, Dokht et al., 2019, Pardo et al., 2019, Mousavi et al., 2020]. Additionally, with the deployment of dense seismic networks for local studies (monitoring of induced seismicity, tomography or study of aftershocks).

This seeks to implement two pre-trained Supervised Deep Learning models (SDL), PhaseNet [Zhu and Beroza, 2019] and EQTransformer [Mousavi et al., 2020], to pick/detect seismic phases in the Colombian territory. Both models were used to pick the seismic phases of the National seismological network (FDSN code: CM), and only EQTransformer was used to pick the seismic phases of two local and temporary networks in Northern South America: The Middle Magdalena Valley seismic array (VMM-Spanish acronyms) and the Caribbean Merida Andes seismic array (FDSN code: YU). The objective is to significantly improve the detection of small, repetitive and/or unusual events that are difficult or impossible to detect using traditional tools or that require the dedication of unavailable personnel.

Once the seismic phases are identified, it is necessary to associate them. Phase association consist to linking phase detections on different stations that originate from a common source. From the seismic phases of the earthquake, the location, and later the magnitude of the event are determined. The automatic association task is predominantly based on a grid search and back-projection algorithms [Sheen and Friberg, 2021, McBrearty et al., 2019b, Yeck et al., 2019]. With the increasing phase picking sensitivity and the large volume of information to be processed, there are other approaches including Machine Learning (ML) and deep learning (DL) [Ross et al., 2019b, McBrearty et al., 2019a, Zhu et al., 2021].

Although ML and DL models are very promising to improve significantly the overall performance of earthquake monitoring workflow, we did not find a user-friendly association algorithm to use, although some recent work has been presented [McBrearty, 2021, Zhu et al., 2021]. Therefore, we use the associator algorithm used by the automatic processing of the Colombian Seismological Network. This is the Scanloc module from SeiscomP3 [Potsdam, 2018]. It is based on DBSCAN to cluster P-phases to make preliminary origins located by the configured locator. Then, adittional P and S phases are aggregated to the existing solution by a relocation procedure. We used LOCSAT and HYPO71 to locate the seismic events. As the Scanloc algorithm was performed on the Colombian Geological Survey computers, it was only possible to use it on the CM and VMM networks, which are the ones they operate. For YU network; we didn't use SGC computers due to data privacy terms in the data, then we used a free association algorithm proposed in the EQTransformer repository and the HYPOCENTER method to locate the seismic events. Finally, the Colombian 1D velocity model [Ojeda and Havskov, 2001] was used herein as input for each locator.

This shows a detailed analysis of the phase picking results of both models and their compatibility with the association algorithms. It also shows the automatic seismological catalog obtained for the three seismic networks. In general, for both PhaseNet and EQTransformer, the automatic national catalogs are similar to the manual one. However, the expected level of earthquake detection detail was not achieved because the association algorithm is very sensitive to false picks. This is a bottleneck, especially for PhaseNet picks. This limitation is substantially reduced for local networks, and therefore, their results show much better resolution. Finally, we merged the automatic catalogs into a single catalog that summarizes reliable information on the seismicity of northwestern South America.

Lastly, through some profiles, we illuminate some actively deforming zones occurring beneath the Northern Andes, mainly bounded by the relative convergence of the Nazca, Caribbean and South American plates. We identified the Benioff zones associated with the subduction of the Nazca and Caribbean plates and we determine the strike direction and dip angle. The catalog shows the prominent discontinuity of seismicity around $5.5°N$, separating the Cauca and Bucaramanga segments [Ojeda and Havskov, 2001, Vargas and Mann, 2013, Syracuse et al., 2016]. In the Bucaramanga segment, two seismic clusters are evident. Bucaramangas seismic nest centered at $6.875°N$ and $73.115°W$ at 150 km depth approximately, and another cluster located at $5.31°N$ and $73.77°W$ close to the municipalities of Ubaté and Cucunubá. Finally, we also illuminate lineaments associated to several systems of active crustal faults, including: -The Magdalena Valley Fault System in the middle of the Eastern and Central Cordillera. - And the Llanos Foothill Fault System at the boundary between the Eastern Cordillera and the South American Shield. To the south of this fault system, there is the Algeciras Fault system. Where a series of earthquake aftershocks were located since the Mesetas-Meta main earthquake (2019-12-24T19:03:52 UTC). And in the north of Colombia and western Venezuela, we identified the triangular Maracaibo Block, limited by the Bucaramanga, Boconó and Ocá fault systems. Based on the above, this implementation is reliable enough to generate automatic seismic catalogs with the appropriate

quality in terms of the event location errors and is capable of defining major tectonic structures.

2 Earthquake monitoring workflow

Considering that we aim to monitor seismic events, we present an ordered recipe to obtain seismic catalogs from the seismological data. First, we show three seismological networks used in this work and how much data is associated to each one. The second section picking seismic phases using two pre-trained deep learning models, and we discuss the theoretical difference of them compared to traditional methodologies. In the next two sections we are going to see how those picks are associated to a single seismic event, and the event located with some traditional methods. Then, we explain the automatic process to compute the moment magnitude for each event. All step by step of the earthquake monitoring workflow used in this work is included in a github repository titled SeisMonitor[1]

2.1 Seismological data acquisition

2.1.1 Seismological data

The times series data and metadata are the principal data to monitor the seismic activity. They are saved according to the standard described in the SEED manual format of the International Federation of Digital Seismograph Networks (FDSN). The time series data represents records of the ground motion and is called a seismogram. In this work, the time series data was saved in MSEED format and is ordered in the SeisComP3 database structure. On the other hand, the metadata refers to the descriptive information of the seismological data, such as the station information and the transfer function of the sensor. Regarding the sensors, they are identified according to the SEED Channel Naming convention (see Table **2-1**). Although there are several ways to save the metadata; in this work, it was saved in DATALESS format.

[1]SeisMonitor: `https://github.com/ecastillot/SeisMonitor`

Table 2-1: Sensor codes.

Sensor	Location	Code	Sampling rate
BB Seismometer	00	HH	100
SP Seismometer	20	EH	100
Accelerometer	10	HN	200

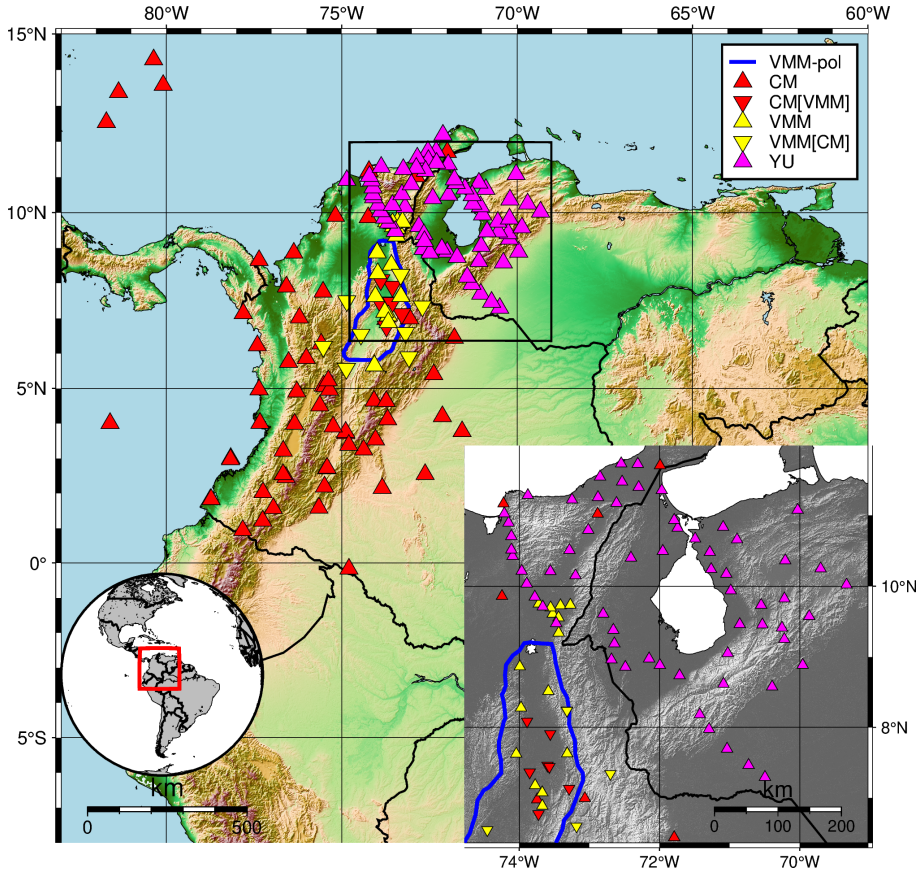

Figure 2-1: Seismic networks: 1. The Colombian Seismic Network (CM) with some stations of the VMM network (CM[VMM]). 2- The Middle Magdalena Valley seismic array (VMM) with some stations of the CM network (VMM[CM]). 3- The Caribbean Mérida Andes seismic array (YU). The blue line represents the VMM polygon

2.1.2 Seismological Networks

The seismological network is the set of stations deployed to cover a region of interest, where the number of stations and the network geometry are parameters to be taken into account for better earthquake locations. We work with three seismological networks to detect and characterize the occurrence of natural seismic activity (figure **2-1**). 1- The Colombian Network with CM network code in the FDSN. This is the national network to monitor seismic activity in the Colombian territory [INGEOMINAS - Servicio Geologico Colombiano (SGC Colombia), 1993]. 2- The Middle Magdalena Valley seismic array. Although this network is also operated by the Servicio Geológico Colombiano (SGC) [Londoño et al., 2019] and then it uses the same network code in the FDSN, in this work this regional temporary array is denoted with VMM network code. 3- Finally, The Caribbean Mérida Andes seismic array with YU network code in the FDSN [Alan Levander, 2016].

Colombian Network (CM)

The Colombian Seismic Network is currently operated by the SGC. Nowadays, until 2021, according to the Colombian FDSN web service[2], this network has one station more than the one reported by [Wielandt et al., 2021]. There are 59 real time public seismological stations with 49 BB and 8 SP seismometers. Also, there are 13 real time public stations with only accelerometer sensors. The figure **2-1** shows that these stations seek to cover the seismic activity that may exist in the Andean zone, the Pacific Coast and the Caribbean zone of Colombia. We downloaded seismic data of this network from 01/12/2019 to 01/01/2021. We also used available data from some stations of the VMM network until 01/09/2020. The data were downloaded by the following sensor priority: First BB seismometers, if not SP seismometers and else finally accelerometers.

Middle Magdalena Valley array (VMM)

As a result of the National Government's interest in developing the exploration of unconventional hydrocarbons using the hydraulic fracturing technique in the Middle Magdalena Valley (Valle Medio de Magdalena - VMM) and La Loma-Cesar, the SGC installed this network to develop a seismicity baseline catalog. This is a local seismic network with temporary BB seismometers along the basin to monitor the seismic activity. Although this network is also operated by the SGC, in this work it is denoted with VMM network code (figure **2-1**). We downloaded the data of 23 temporary seismological stations from 01/01/2016 to 01/09/2020. Furthermore, for a better resolution in the earthquake detection, in this period we also downloaded available data of other 9 public stations of the CM network that surrounded the basin.

Caribbean Merida Andes Seismic array (YU)

The Caribbean- Mérida Andes (CARMA) seismic experiment was developed to investigate the flat slab subduction and plate edge tectonics in Northern South America. This temporary seismic array has 65 temporary BB stations deployed in North-Western South America (NWSA) zone from 2016 to 2018. The figure **2-1** shows the network geometry around Colombian and Venezuelan territories. We only downloaded the one year approximately (01/01/2016 to 01/02/2017) from the CARMA FDSN web service[3] .

[2]FDSN web service of the Colombian Seismic Network: `http://sismo.sgc.gov.co:8080/`

[3]FDSN web service of the Caribbean- Mérida Andes (CARMA) seismic experiment: `https://www.fdsn.org/networks/detail/YU_2016/`

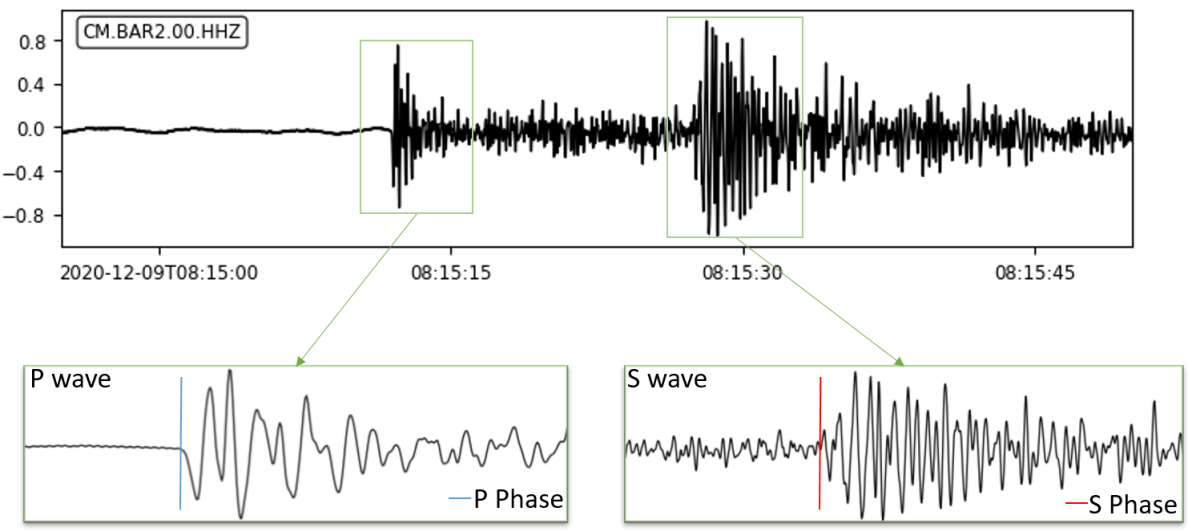

Figure 2-2: The upper panel represents a normalized seismogram of an earthquake. The figures below show the timestamp corresponding to each P and S seismic phases of the event.

2.2 Phase Picking

2.2.1 Seismic body waves

A seismic event is a sudden movement produced by a rupture process that releases energy in the form of elastic waves, which travel through the Earth's medium, reflecting and refracting on the different types of materials they encounter in their path. Seismic waves are mainly divided into two groups: body waves and surface waves. For the purposes of this investigation body waves are explained: P-waves and S-waves.

P waves

It is a longitudinal wave whose oscillation is in the direction of propagation, that is, the medium in which it travels is alternately compressed and dilated in the same direction of the propagation. Figure **2-2** shows the first transient record of the seismogram alluding to its name as primary wave, it travels faster than the S-wave.

S waves

The S-wave or secondary wave is a transverse wave that oscillates perpendicularly to the direction of propagation. Generally, these oscillations produce most of the damage when a seismic event occurs. Figure **2-2** shows that it is the second transient recording. In general terms, P and S wave recordings compose the main local signal of a seismic event.

2.2.2 Seismic arrival times

P and S waves are recorded in the seismogram; now to monitor seismic activity, it is necessary to detect the arrivals of each seismic wave. These arrivals are called seismic phases. The figure **2-2** shows the timestamps corresponding to each P and S seismic phases.
Seismological analysts are trained in recognizing seismic phases (mainly P and S seismic phases) and they know some mechanisms to detect seismic phases at each seismic station of each type of seismic event. For example, the use of signal filters could help to smooth the signal at the appropriate frequencies in order to detect the changes in amplitude of each arrival.
For dense seismic networks or for long seismic processing times, detecting and picking seismic phases could be a really difficult task in terms of time and dedication. Therefore, there are efforts to automate this process. Among them one of the most prominent is the STA/LTA [Allen, 1978]. As shown in Figure **2-3**, this algorithm is based on using two windows; one short ("Short term average"-STA) and a longer one ("Long term average"- LTA), to calculate a rate between the average amplitudes of each window. Once this rate is calculated, if it exceeds a certain threshold then the arrival of a seismic phase is detected. Before calculating the ratio, it is necessary to use a filter to improve the signal-to-noise ratio to facilitate the detection of the amplitude change. There are several studies that used this method and obtained good results [McEvilly and Majer, 1982] [Earle and Shearer, 1994]. Moreover, there are improvements to this method [Baer and Kradolfer, 1987]. On the other hand, it was developed AR-AIC picker [Sleeman and van Eck, 1999], it applied joint autoregressive (AR) modelling of the noise and seismic signal and Akaike Information Criterion (AIC) to determine the onset of a seismic signal. Furthermore, some algorithms analyze wave polarization to pick S seismic phases [Cichowicz, 1993] or to improve S-wave arrival time measurements [Ross and Ben-Zion, 2014]. Other algorithms adopt wavelet transform to pick P and S seismic phases [Anant and Dowla, 1997] [Al-Hashmi et al., 2013].
Despite the substantial efforts outlined above, these algorithms have multiple limitations that make the process not fully automatic and not as accurate as that of an experienced analyst. For example, the STA/LTA algorithm has been used for a long time in the SGC with some problems including: - it sometimes confuses P and S phases, - it doesn't pick seismic phases for low SNR in the seismic signal - it confuses noise peak signals with seismic phases. Besides, it needs the adjustment of the mentioned filters, time windows or thresholds according to the noise level of each station. For all these reasons, in this work we were motivated to find new algorithms that improve the effectiveness of the automatic detection and picking systems.

2.2.3 Phase picking with deep learning

Our goal is to use an algorithm that can be general enough to pick seismic phases regardless of the station where it is recorded or type of earthquake occurring. Something similar to how a seismological analyst does it, but this time in an automatic way. According to the concept defined by International Business Machines Corporation (IBM), *Machine learning (ML) is a branch*

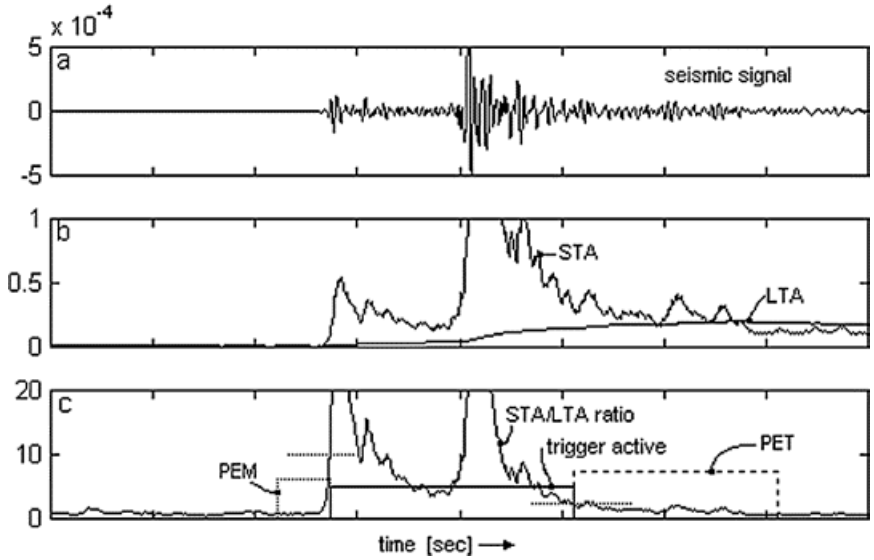

Figure 2-3: STA/LTA detection algorithm. Taken from [Marmureanu, 2009]

of artificial intelligence (AI) and computer science which focuses on the use of data and algorithms to imitate the way that humans learn. In this sense, we focused our approach in a type of machine learning based on artificial neural networks, which it is called Deep Learning (DL).
ML models can be designed as supervised learning (SL) models or as unsupervised learning (UL) models. As the names suggest, the difference between them is the way of learning. The first one uses labeled data sets to train algorithms to classify data and predict outcomes, then the machine can learn if the model prediction is similar to the label. On the other hand, UL models don't use any labels or explicit instructions on what to do with it. It identifies patterns in the structure of the input data set, something similar to self-learning. Although, UL could perform more complex tasks than SL, they are more unpredictable. Besides, we want to take advantage of large labeled data sets provided to pick seismic phases [Mousavi et al., 2019] [Magrini et al., 2020]. Therefore, we focused our work to make predictions with two pretrained Supervised Deep Learning (SDL) models.
We also direct our work in this sense because there are several promising results in the use of SDL models applied to seismic phase picking. To understand how they work and how they are evaluated, we present five general steps that any SDL model follows.

1. Prepare the data. Neural network models require numerical labeled data as input for training and testing. DL phase picking models use seismic signals as input data; and normally for each given input, the network outputs the probability of an P-phase, an S-phase, or noise for each time sample within the seismic signal window. The Stanford EArthquake Dataset [Mousavi et al., 2019]; a global data set of seismic signals for AI, is one of the state-of-the-art data sets to prepare seismic signals for DL phase picking models.

2. Define the model. The neural network model is an architecture defined by DL layers

widely used to extract high-level abstract features, increasing the data interpretability to make desired predictions. There are several neural networks, the most frequently used for earthquake monitoring workflow are as follows: Multilayer Perceptron (MLP), also known as multilayer feed-forward network, normally used at the end of the model architectures to classify the data. Convolutional Neural Networks (CNN) are able to successfully capture the spatial and temporal dependencies of the data to extract high-level abstract features. Residual Neural Networks (ResNet) use skip connections to jump over layers to simplify the architecture and accelerate the learning speed. Recurrent Neural Networks (RNN) are used to create a persistent memory of data, then they are very useful to understand high level abstract features in sequence of data. Transformer networks adopt the mechanism of self-attention to prioritize each part of the input data. Finally, Graph Neural Networks (GNN) use graph theory; where a graph is defined as a set of nodes with specific features and edges to represent node connections, to extract high-level abstract shared features at the nodes based on the node connections. This neural networks overview, allows us understand the basic idea intended by each layer presented in the different model architectures.

3. Train the model. The training process refers to fitting the model parameters provided by each layer to generate good predictions. It requires defining a loss function and an optimization algorithm. The loss function is a metric to judge when the model makes bad predictions, and the optimization algorithm seeks to minimize the loss function by iteratively executing of comparing several solutions (different parameter weights) until a satisfactory solution is found. The binary cross-entropy loss is commonly used for binary classification. Then Phase picking DL models normally use it to predict binary vectors to obtain the probability functions. On the other hand, ADAM optimization algorithm is one of the most used for DL applications.

4. Evaluate the model. Once the model has been fitted, it must be evaluated against the test data set. Once the test data set predictions have been obtained from the model, the next values are computed:

   - True positives (T_p): Predicted positive and are actually positive.
   - False positives (F_p): Predicted positive and are actually negative.
   - True negatives (T_n): Predicted negative and are actually negative.
   - False negatives (F_n): Predicted negative and are actually positive.

   The model could then be judged with the usual evaluation metrics defined as follows:

$$Precision = \frac{T_p}{T_p + F_p} \tag{2-1}$$

$$Recall = \frac{T_p}{T_p + F_n} \tag{2-2}$$

$$F1 = 2 * \frac{Precision \times Recall}{Precision + Recall} \tag{2-3}$$

Precision computes the percentage of positive instances out of the total predicted positive. Recall computes the percentage of positive instances out of the total actual positive instances. And F1-score is the harmonic mean of precision and recall, where higher F1 scores, the better is the model. Normally, F1-score is the selected metric to evaluate DL models presented in the earthquake monitoring workflow.

5. Make predictions. If the model works as well as the user requires, the model is ready to make predictions on any prepared data set.

With the aforementioned, we are going to introduce some of the phase picking SDL models and establish why we chose EQTransformer [Mousavi et al., 2020] and PhaseNet [Zhu and Beroza, 2019] pretrained models to pick seismic phases on the Colombian seismological data (PhaseNet only was applied to CM network).
Phase Picking SDL results are obtained from shallow neural networks [Dai and MacBeth, 1997] [Gentili and Michelini, 2006], however their performances were greatly limited by its simple neural network architecture, little number of training examples and slow computational speed. Phase Picking SDL models have increased substantially due to the emergence of CNN. One of them was developed to P wave arrival picking and first motion polarity determination [Ross et al., 2018a]. Next, ConvNet SDL model was trained to detect seismic body-wave phases with millions of hand-labeled phases from analysts at the Southern California Seismic Network (SCSN) [Ross et al., 2018b]. The model's input data consists in three-component records with a length of 400 samples and it classifies this record according to its detection as P,S or noise windows. Its results suggest that it is extremely sensitive and robust in detecting phases even when masked by high background noise.
PhaseNet SDL model was presented to pick the arrival times of both P and S waves [Zhu and Beroza, 2019]. The model input data consists of three-component records with a length of 3001 samples and it uses an adapted version of the U-Net architecture [Ronneberger et al., 2015]; a specific CNN architecture to create a segmentation mask. Each input data is tagged as a probability function with probability 0 when there are not seismic phases or else a gaussian function is created, where P and S seismic phases are set with a probability of 1 at the first arriving P and S wave (figure **2-4**-b). It was trained with six hundred thousands records approximately and tested with about eighty thousands records taken from Northern California Earthquake Data Center Catalog (NCEDC). Its results provide high accuracy and recall rate for both P and S picks, and achieves significant improvement compared with a traditional STA/LTA method.

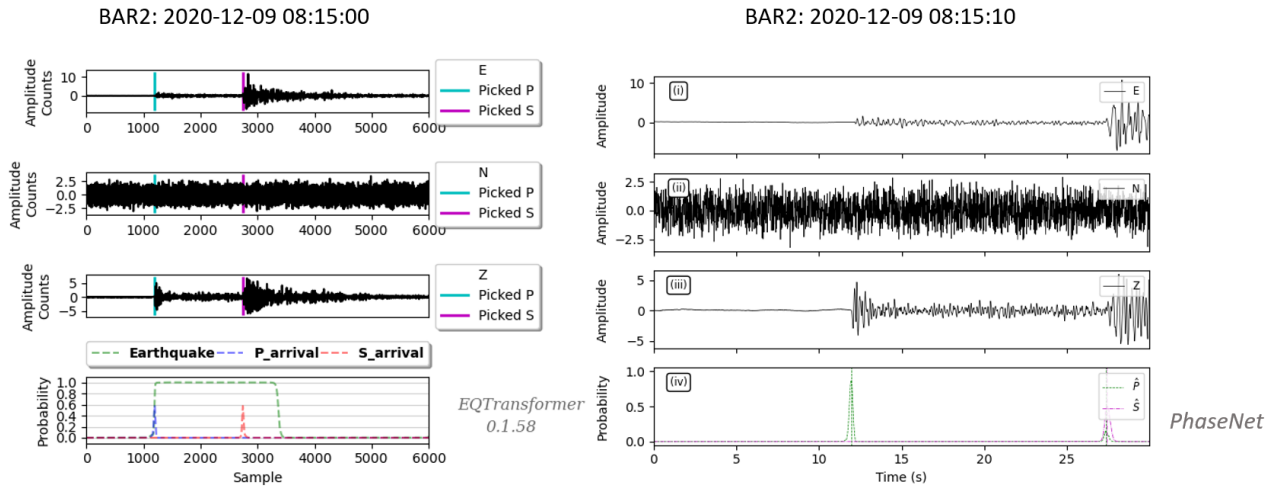

Figure 2-4: EQTransformer and PhaseNet Supervised Deep Learning pre-trained models to pick seismic phases.

PhaseNet's approach served as one of the inspirations for the following SDL model. Other CNN was designed with the same labeling approach for classifying seismic phase onsets for local seismic networks [Woollam et al., 2019]. Even though they used a single 1D waveform as input data and they didn't have extensive training data, they demonstrated phase picking improvements in comparison with STA/LTA method. Furthermore, Cospy SDL model proposed other CNN architecture approach to picking seismic phases to solve two Phasenet architecture drawbacks [Pardo et al., 2019]. It receives 1024-sample as input data and was trained with a large amount of data to perform P and S phase picks separately. Its results try to reach the human-level performance and can contribute to decreasing the need for manual analysis.

Other ConvNet SDL was developed to achieve an automatic seismic event and phase detection [Dokht et al., 2019]. With the help of the CNN architectures, it was done in two steps: first to separate earthquake from nonearthquake and second to discrimanate P and S waves. They identify $\sim$ 20% more events than manual event detections and provide initial estimates of phase onset times to determine preliminary earthquake locations to monitor natural and induced seismicity. Besides, PickNet SDL model was presented to pick P and S wave arrival times with high accuracy close to that human experts [Wang et al., 2019], and it was used to determine seismic tomography and contribute to improve the understanding of the Earth's interior structure. PickNet architecture was designed with CNN and ResNet to speed up the training convergence and refine the detection result, and it was trained with a large amount of High-sensivity Seismic Network (Hi-net) data to perform P and S phase picks separately. In contrast to the other SDL models, their data was collected of local earthquakes with epicentral distances up to $\sim$ 1000 km. They obtain $\sim$ 10 times more P and S phases than reported by Japan Meteorological Agency (JMA), and the predicted picks were used to perform a tomographic inversion to successfully illuminate the Japan subduction zone.

The above approaches use DL models to extract high-level features to pick seismic phases. However, EQTransformer SDL model was proposed for simultaneous earthquake detection and phase picking [Mousavi et al., 2020] to improve the model performance. The input data is 6000 samples of three-component seismograms and there are three output sequences representing probabilities associated with the existence of the earthquake signal (detection), and the P and S arrival times. The detection output is a box-shaped function and the pick detection outputs are triangular functions to define the probabilities of P and S phases (figure **2-4**-a). The architecture is designed with a central encoder and three decoders, it uses a global attention mechanism at the end of the encoder to direct the attention to the earthquake signal, and it also uses a local attention mechanism in two decoders to direct the attention for both P and S phases. This new approach is inspired by how the seismological analyst conducts it. First, their attention is focused in detect the event; and then, they proceed to pick seismic phases. This SDL model was trained with different and large number of seismic traces from different regions reported in STEAD [Mousavi et al., 2019]. Furthermore, it employs augmentation techniques to simulate several different types of seismograms usually recorded in continuous data. EQTransformer was evaluated on aftershock series from Japan data unknown to the model and was able to greatly increment the number of picks reported by JMA.

All of the above allow us to recognize the high influence of DL on phase picking. Although we are aware of the good results presented in each one of them, we only find well-documented code for PhaseNet and EQTransformer. Besides, according to the results in a common test data set from STEAD, we could assume that these two are the best and the most recognized SDL models in the picking phase state of art [Mousavi et al., 2020]. Therefore, we focused our phase picking approach using two pre-trained deep learning models: PhaseNet and EQTransformer.

2.3 Phase Association

Phase association consists to linking phase detections on different stations that originate from a common earthquake. Seismological analysts associate detections to the same seismic event when these are close in time and, initially, come from stations spatially close (figure **2-5**). The other seismic phases will be associated along the way checking that the phase residuals or uncertainties in hypocenter location do not increase dramatically.

Although the association concept is simple, it is a really hard task to address it automatically because it needs to cluster coherent phases and removes the false ones. Besides there can be various origins of seismic signals in the same interval of time; even overlapped. Which in turn could be provided from the same or different hypocenter locations.

In general, automatic phase association is predominantly based on a grid search and back-projection algorithms [Sheen and Friberg, 2021, McBrearty et al., 2019b, Yeck et al., 2019]. The region of interest is discretized, and for each grid the detected arrivals are back-projected and stacked to search a grid that exceed a threshold of count of back-projected arrivals. If one of

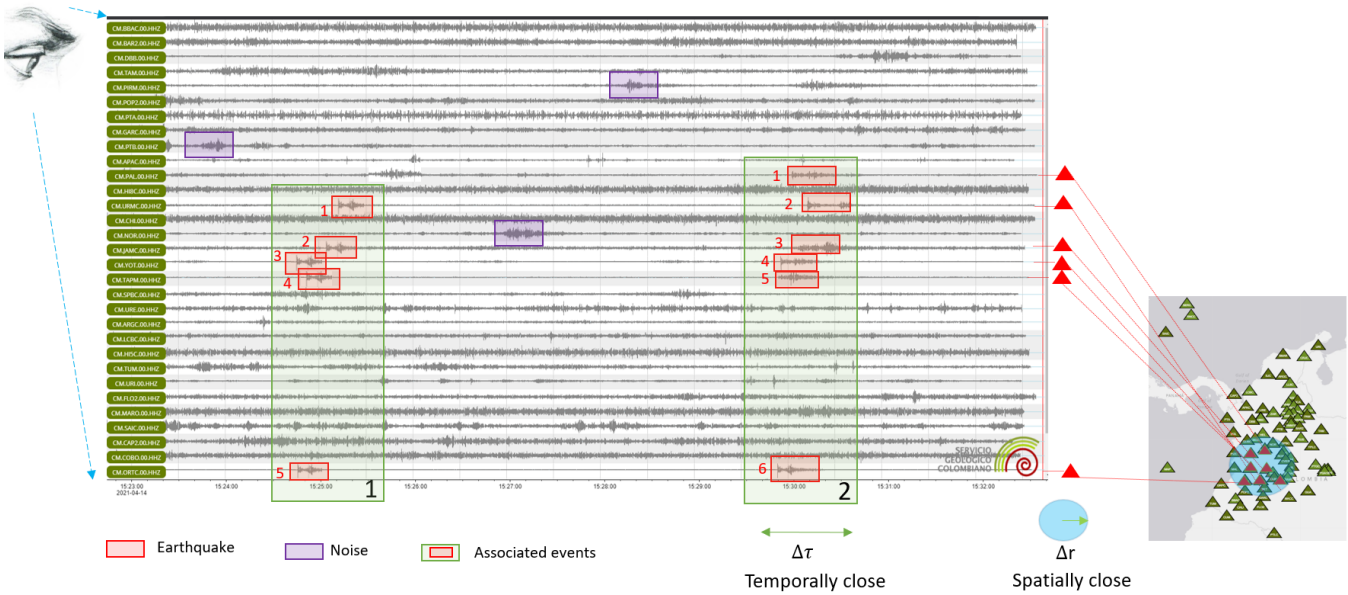

Figure 2-5: The association algorithms seek to cluster the detected events by each station that record the common earthquake. Normally, the detections are close in time and, initially, come from stations spatially close.

them exceeds, the algorithm assumes a coherent origin. On the other hand, with the increasing phase picking sensitivity and the large volume of information to be processed, there are other approaches thanks to the notably ML and DL progress [Ross et al., 2019b, McBrearty et al., 2019a, Zhu et al., 2021].

Although ML and DL models are very promising to improve significantly the overall performance of earthquake monitoring pipelines, when we looking for a phase associator, we did not find a user-friendly documentation. For this reason and because we aim to use the same phase association for comparison, we use the scanloc module from SeisComP3 [Potsdam, 2018], the associator algorithm used by the SGC. We use it to associate seismic phases obtained in the CM and VMM networks. However, as YU seismic network is private, we couldn´t use scanloc for this purpose. Therefore, as YU network has stations located relatively close to each other, we use the association algorithm proposed in the EQTransformer repository.

The EQTransformer-associator algorithm is a very simple algorithm based on the detection times. The scanloc module is based on the DBSCAN algorithm, that at first clusters P-phases. Next, it is based on a grid-search algorithm and back-projection method to locate the clusters and get preliminary origins. Finally, it associates additional picks from P and S waves by a relocation procedure. P phases are added if travel-time residuals are not larger than a user-fixed threshold. Additionally, S phases are added if 1) The reference P phase is already associated and 2) if the root mean square (RMS) travel time residual is not larger than an user-fixed threshold.

2.4 Event location and magnitude estimation

Once we have identified the set of phases that correspond to a common seismic event, we have to get the earthquake location (X, Y, Z) and the origin time T in which it was nucleated. Therefore, there are four unknown earthquake parameters that will have to be estimated from the observed arrival times. This is known as the inverse problem.
On the other hand, the forward problem consist to predict travel time t^i_{pred} for each i^{th} station considering prior knowledge of the location and time origin of the earthquake $m = [X, Y, Z, T]$, the velocity model of the area, and the location of the stations. We could get the predicted travel time t^i_{pred} means of ray-based methods, which solve the kinematic ray equation, or grid-based methods, which solve the Eikonal equation [White et al., 2020].
However, as we mentioned before, we want to find the optimal solution for m from the observed arrival times t^i_{obs}. Normally, it is obtained when the smallest arrival time residual is found at each station. The residual r_i at the i^{th} station is defined as the difference between the observed travel time t^i_{obs} and predicted travel time t^i_{pred}.

$$r_i = t^i_{obs} - t^i_{pred} \tag{2-4}$$

The most widely used algorithms to identify the best fitting event are based on a grid search approach in combination with iterative least squares inversion algorithm [Micallef, 2019].
As we suggested in the section 2.3 regarding the Scanloc module, after the first P-clusters are collected then a grid-search algorithm is used to locate the events. In this process, once the region is discretized, potential locations are founded in each grid point computing the P-residuals. Then, any earthquake location program is launched. For this purpose, we used LOCSAT, HYPO71 to locate the seismic events corresponding to the CM and VMM seismic networks. Each of these earthquake location programs determine the best-fitting location in the possible potential locations by using iterative least squares inversion algorithm until the RMS is sufficiently minimized. This location process is continuously repeated while the other P and S phases are associated. In the YU network, the HYPOCENTER location program provided by the SEISAN software was used to locate the clusters given by the EQTransformer-associator algorithm.
In order to quantify the energy released by the seismic events, the instrument response is removed from windowed seismic data on each station. Then, thanks to the Scamp Seiscomp module, the amplitudes were computed from waveform data based on incoming associated picks to estimate the magnitude of the seismic events. The SGC computes local magnitude M_L for magnitude values smaller than $M_L = 4$. For those cases, it is estimated according to a distance-correction function calculated for five zones due to the different attenuation values associated with the various tectonic environments and regional geological features present in the country [Lopez et al., 2020]. However when the magnitude values are greater, the moment magnitude M_w derived from m_B magnitude [Bormann and Saul, 2008] is preferred.
On the other hand, we always calculate the moment magnitude M_w derived from m_B magnitude for CM and VMM networks. So far, for the YU network, we have not calculated the magnitude.

Although both, the SGC and this work, used different magnitude types for magnitude values smaller than $M_L = 4$, one of the biggest reasons to divide the territory into zones is to decreasing discrepancies with M_w. Therefore, we can compare the magnitude values of the manual and automatic catalogs.

3 Phase picking results

This chapter is dedicated to show the phase picking results, processing time results, some specific examples to elucidate and some analyses to evaluate the performance of the SDL pre-trained models. For this purpose, we only analyze the phase picking results of the CM network because it is the only one from which we have analyst picks to compare to.
First, we present the processing time to run PhaseNet and EQTransformer models in the CM network data. Also, we show the versatility of the two models. Second, we show some examples of both SDL models where we obtained very good results to detect seismic phases in earthquake aftershocks. Third, we present the entire catalog phase picking results. We study the threshold probability of each station in terms of generating good phase picking results. To achieve this, we look for EQTransformer and PhaseNet picks that are in the manual pick database. In principle, the picks that are found in both catalogs (SDL and manual) give us an idea of the probability threshold of the SDL that best reproduces the manual picks. Besides, this analysis was made for three types of instruments: HH, EH and HN. Finally, for picks founded in both catalogs, we analyze phase picking time precision and true phase probability distributions. All of the above gives a general idea of the advantages and disadvantages of using EQTransformer and PhaseNet models on seismological data from a regional network.

3.1 Processing times

For the CM network we ran EQTransformer and PhaseNet SDL pre-trained models in 30 free jupyter notebook environments from Google Colaboratory. Each jupyter notebook offers the same computer device: Intel(R) Xeon(R) CPU @ 2.30GHz (1 core, 2 threads) and RAM: $\sim 12.6GB$. In each of these we download and process the data every 2 separately hours for a total of 395 days of 59 seismological stations and 13 accelerometer stations. Throughout the year and one month of processing data not all stations operated continuously. PhaseNet was executed with the following input hyperparameters: 50% data overlap and 0.3 P-phase and S-phase probability thresholds. And EQTransformer was executed with: 30% data overlap, 0.3 detection threshold and 0.01 P-phase and S-phase probability thresholds. The batch size used in both model was 100 examples. Unlike EQTransformer, PhaseNet outputs are given in sample units for each segment, we then converted them to time. To do this, we had to study the overlapping segments and keep the segment with the highest average probability. This small amount of post-processing is also considered in the time taken by the algorithm.

EQTransformer took ~ 5 minutes to process 2 data hours in 1 Colab jupyter notebook, while PhaseNet took ~ 9 minutes. Then, 2 data hours take ~ 14 data processing minutes for both models. Although both models process the same length of data, in a single run PhaseNet can only receive half as much data as EQTransformer as input, then, PhaseNet took longer time. Furthermore, PhaseNet overlaps more data. Considering the above, processing 395 days of data from 72 stations using both models in 30 Colab jupyter notebooks takes approximately 2 days.
The SGC hires expert seismological analysts to process and disseminate real-time information from the public stations of the CM network. Informally, we asked them to estimate the time it would take an analyst to manually process 2 hours of data. Although there are many factors that can vary the result (emotional conditions, active breaks, earthquake density, active stations, etc.). On average, a processing time of ~ 1.3 hours per 2 hours of data is considered. Under this very shallow approximation, an expert will take ~ 304 days to process 395 days of 75-stations data.
Therefore, both models can reduce processing times considerably and even be speeded up if better hardware is used if you have better hardware than the one presented in this investigation. Furthermore, they are flexible in terms of hardware and software components. This makes it very functional and operative in any system where seismological processing is required.

3.2 EQTransformer and PhaseNet performance

3.2.1 Introduction to general examples

Both models have their advantages and disadvantages, we present some specific examples to illustrate each of them. The example presented in the figure **3-1**a shows an intermediate depth seismic event where P-phase and S-phase were detected by all pickers. The event was detected in the closest station to the hypocentral location (BAR2 to $\sim 0.13°$ of distance, where S-P time difference is about 15 seconds), and was located in the Bucaramanga Nest, a zone with significant seismic activity in a very compact volume [Prieto et al., 2012].
Figure **3-1**b shows again an intermediate depth seismic event but this time located at a site far from the station. the S-phase was not detected by PhaseNet. This happened because the S-P time difference is larger that the time window that PhaseNet receives as input. Therefore it can not cover the entire waveform record to predict correctly. Similar cases were detected in the seismic events produced in the Bucaramanga Nest. Stations farther away than $\sim 2.5°$ have more than 30 seconds of S-P time difference. Therefore, PhaseNet can not pick seismic phases correctly in several stations that record a Bucaramanga nest seismic event. However, for the closer stations, it can detect the seismic phases very well, even events not detected either by the analyst or by EQTransformer (Figure **3-1**c).
As we suggested before, sometimes PhaseNet can detect seismic events not detected by other methods. This situation is even more pronounced when the seismic events are shallow and

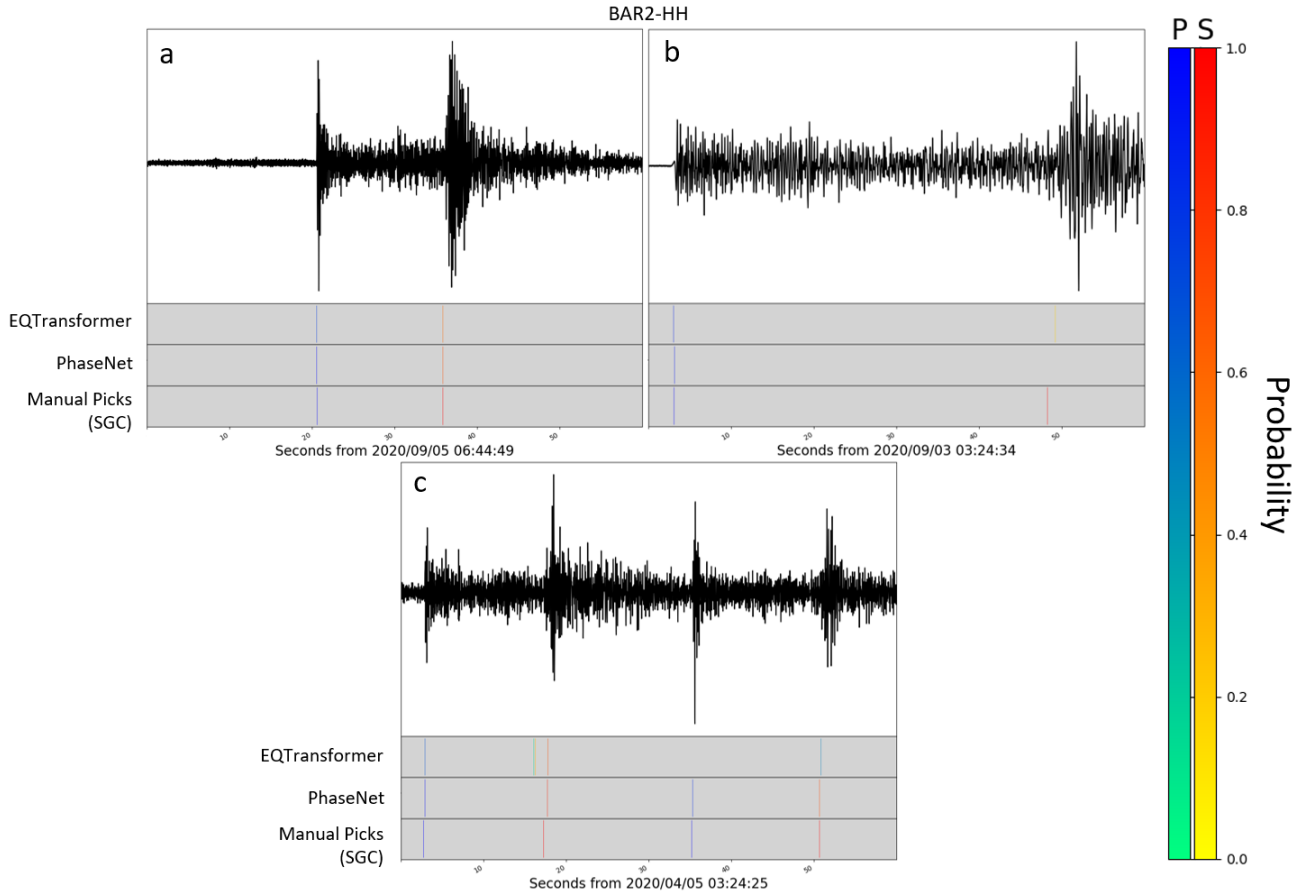

Figure 3-1: Examples of advantages and disadvantages of the EQTransformer and PhaseNet models. a) EQTransformer, PhaseNet and seismological analysts detect all phases recorded at station BAR2 as a result of an earthquake located in the Bucaramanga nest. BAR2 is the first station to record the earthquake. The time difference S-P is usually 15 seconds. b) PhaseNet can not detect the S phase for an event where the time difference S-P is larger than 3000 samples (> 30 s). c) Two consecutive seismic events in the Bucaramanga nest. Unlike, EQTransformer, PhaseNet could detect all seismic phases.

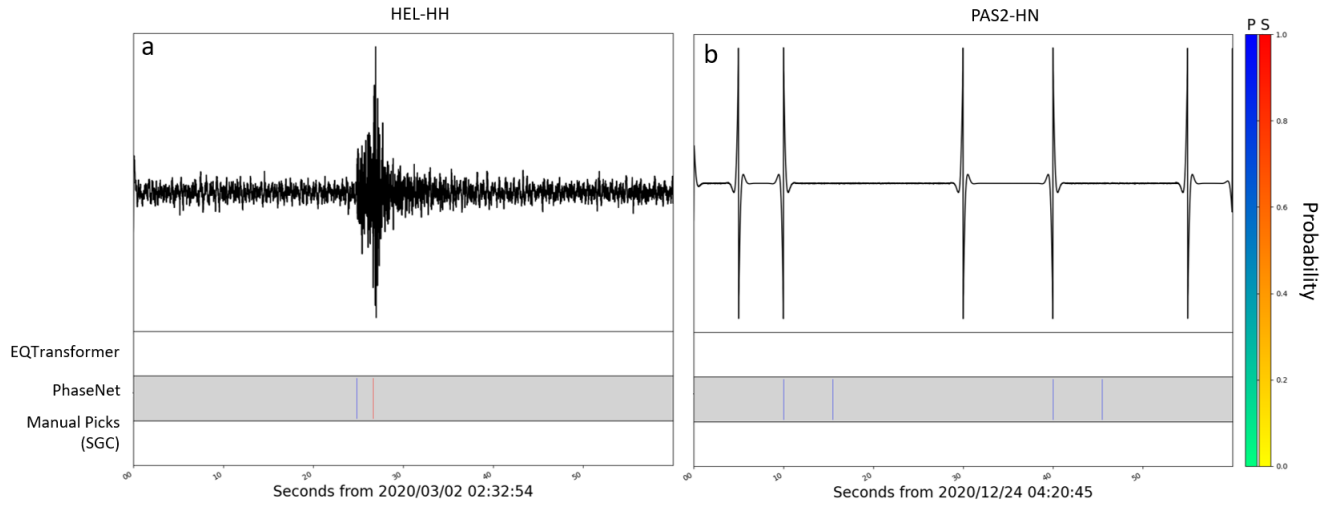

Figure 3-2: Introduction to PhaseNet results. a) PhaseNet is sometimes the only one that can detect very small events. b) PhaseNet often confuses spike signals with P phases.

have small amplitudes (Figure **3-2**a). These events are usually seen in one or two stations of a regional network such as CM. Although we are aware about this advantage, in this regional seismic processing it is not very useful as they cannot be located. On the other hand, in figure **3-2**b we note that PhaseNet makes several mistakes for spike signals and filtering them is a really hard task because the probability values are very high.

A final example (figure **3-3**), shows a set of earthquake aftershocks. We analyzed 8 minutes of data 5.5 hours after the main shock (not shown) at the station closest to the epicenter ($\sim$ 32 km of distance). The main shock origin time was 2019-12-24T19:03:52 UTC and its magnitude was 6.0. The epicenter location was in Mesetas-Meta (lat:$3.45°N$, lon:$74.19°W$) and its depth was 8 km [Mayorga et al., 2020, Londoño et al., 2019, Prieto, 2022].

EQTransformer and PhaseNet models can detect events not detected by the seismological analyst. In this interval, both manage to register more events than reported by the SGC. EQTransformer finds 3 adittional events while PhaseNet finds 5. Notwithstanding the above, PhaseNet predicts more false positives than EQTransformer. However, this can be managed for both models by setting probability thresholds.

3.2.2 Truthfulness of the picks results

In figure **3-4** we show the P-phase picking results of both models together with manual picks in the CM network. PhaseNet has much more picks because it has some false picks attributed to signal spikes or sometimes because it confuses P and S seismic phases, among others. In addition, the most drastic changes in the scale of picks for both models occur at the stations with accelerometer instruments (HN sensor). This means that in these instruments there is a higher probability of false picks. We will discuss this in more depth later.

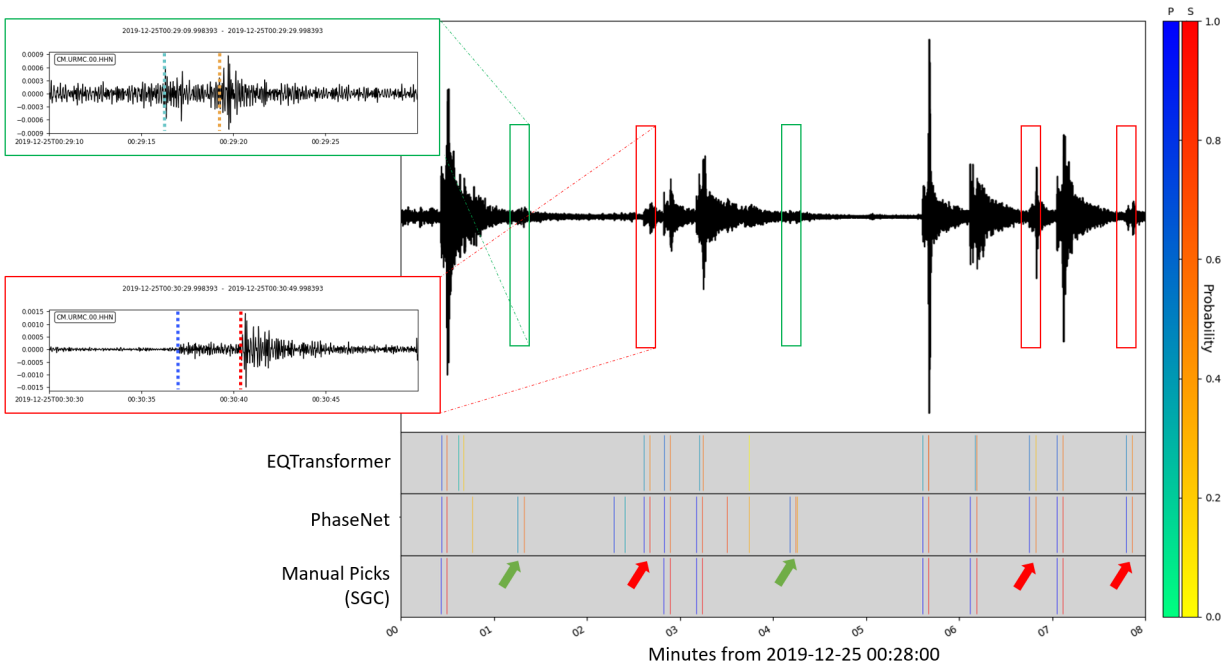

Figure 3-3: Autopicking algorithms applied to a set of earthquake aftershocks. The studied time interval was 8 minutes, 5.5 hours after the main shock (M 6.0) at the station closest to the epicenter ($\sim$ 32 km of distance). Red squares represent events detected only by EQTransformer and PhaseNet. Green squares represent events detected only by PhaseNet.

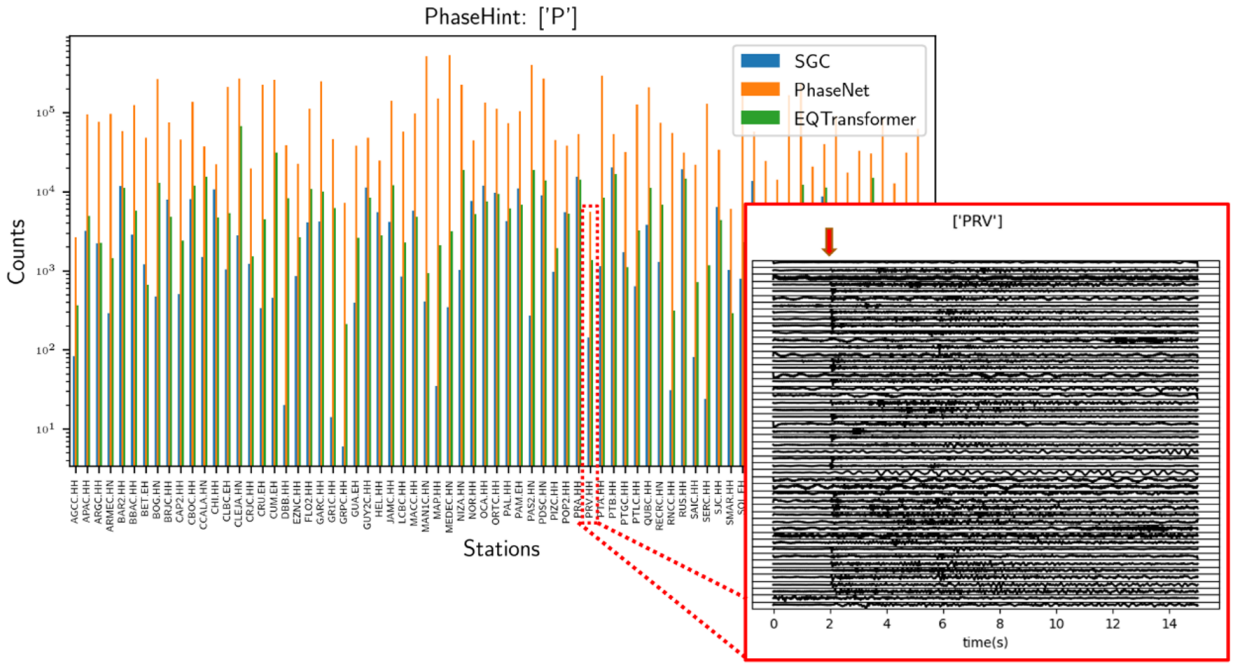

Figure 3-4: Comparison of picks reported by SGC, PhaseNet and EQTransformer models. EQTransformer model complements the database of *isolated stations* such as the PRV station. We present some random PRV phase picking results at 2 seconds in a 15-second time window. We find out the majority are true picks because there were noticeable amplitude changes.

On the other hand, EQTransformer keeps approximately the same scale of picks as the manual ones. EQTransformer has more picks in some *isolated stations*. Where the seismic events are only observed at one station because the seismic event is small and close enough, or because there is not much station density. In these specific cases it would be normal for the analyst not to see or attempt to pick the earthquake .

For instance, both situations occur at PRV station (lat:13.376, lon:-81.36). It is an isolated station located in the Providencia Island (in the Caribbean 5 degrees north of continental Colombia). To get a general idea of what happened here, we chose random waveforms from these specific cases and plotted them aligned at 2 seconds in a 15-second time window (Figure **3-4**). We find out that the majority are true picks because there were noticeable amplitude changes. Then, even for these cases, EQTransformer complements the database.

Assuming that the SGC have all the seismic phases, we denominate true picks when we find the respective EQTransformer or PhaseNet pick in the SGC database. The time threshold condition to join the picks are if the time difference between them is less than 1.5 seconds. In order to refine the results, we study the probability threshold to have true picks.

In figure **3-5** we show a representative example of the general probability behavior of both models for both P and S phases in HH instruments. Most EQTransformer picks turn out to be

true picks. It is shown to be robust across the full width of probabilities. For both P and S phases, from probability $\sim 0.05 - 0.15$ there are more true than false picks. This makes it very reliable at high probabilities. Curiously, for the S-phases predicted by EQTransformer in figure **3-5**, apparently there are more false than true picks for the highest probabilities ($\sim 0.85 - 1$). We claim these picks really do exist, they just do not exist in the SGC database.
On the other hand, PhaseNet results suggest that the model is very sensitive in terms of probability values; that is, we only trust on very high probabilities. As we mentioned before, PhaseNet delivers a large amount of picks. Therefore, in terms of good quality in the seismic processing task, for PhaseNet we need a more robust associator algorithm than could be used for EQTransformer. Because apart from associating the picks in different events, it must also be sufficiently prepared to be able to separate true picks from many that are false. However, as we are going to show in the section 4.1.1, another solution is to remove those picks by probability thresholds before using the association algorithm.
In addition, we are also interested in presenting the same analysis for different instruments. EQTransformer maintains its good performance for EH instruments. While those of PhaseNet seem not to be as good as those shown for HH. We expect this result because the EQTransformer model was trained with a large number of EH signals compared to the PhaseNet model. For this reason, it was able to better generalize the detection on this type of signals.
Regarding HN instruments, as its data have different sampling rate as the data with the models were trained. EQTransformer interpolates them at 100 Hz, and then, runs along the data trimming at 6000 samples. Therefore, the model always is trying to predict 1 minute of data (as in the training). PhaseNet does not interpolate by default. It only runs the data trimming at 3000 samples. Hence, PhaseNet is only trying to predict 30 seconds of data when the sampling rate of the signal is 100 Hz. However, PhaseNet allows the user interpolate at 100 Hz. But, we realized this too late. The user must infiltrate the code and adjust his own data preprocessing [1].
Consequently, we pass the data with PhaseNet's default preprocessing settings. That is, in our processing, PhaseNet for accelerometers is trying to predict results every 15 seconds instead of the usual 30 seconds (as in the training). Of course, this is not desired. Then, we do not focus the results on the comparison of models to predict on accelerometer signals. However, we are going to discuss them separattely.
In figure **3-7**, EQtransformer interpolation proves to be a very useful engineering artifact for predicting results in accelerometer signals. This means that even if the model has not been trained with accelerometers, it still has good predictions. For PhaseNet, we recommend interpolating the data. Surely, this will allow to show better results.
We compare the temporal closeness of the automatic picks with the manual picks. We can only do this analysis for picks found in both databases. In general, the models pick the seismic phases at the same time that the analyst do (figure **3-8**). However, the pick time differences are larger as the pick probabilities are smaller. This mainly happens for S phases.

[1] "*You can customize the preprocessing of mseed file, such as filtering and resampling, inside the function* $read_mseedindata_reader.py$."

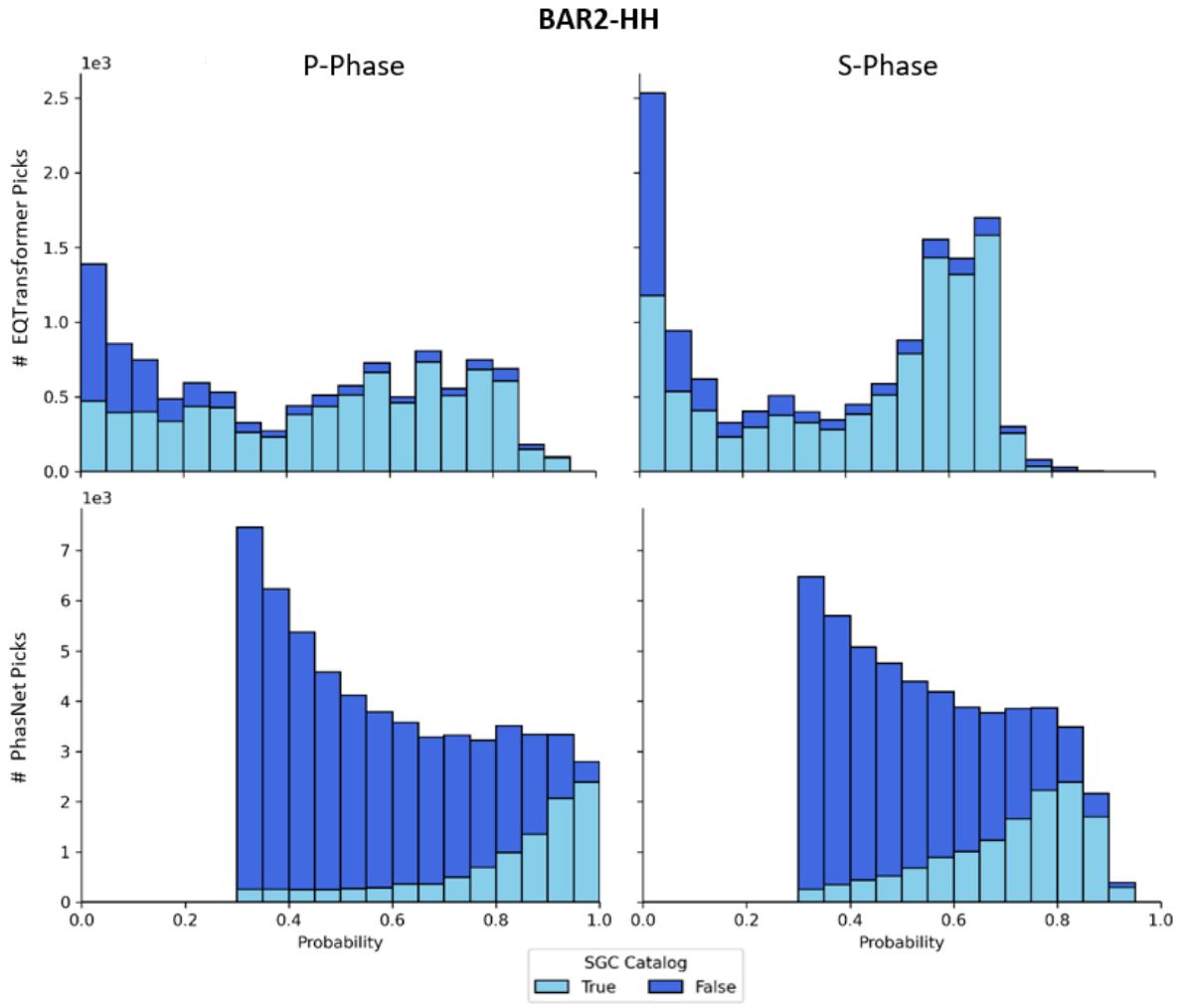

Figure 3-5: Stacked number of P and S picks as function of EQTransformer and PhaseNet probabilities for BAR2 station (HH instrument). The light blue bar represents the number of picks that were found in the SGC database. While the dark blue bar represents those that were not found.

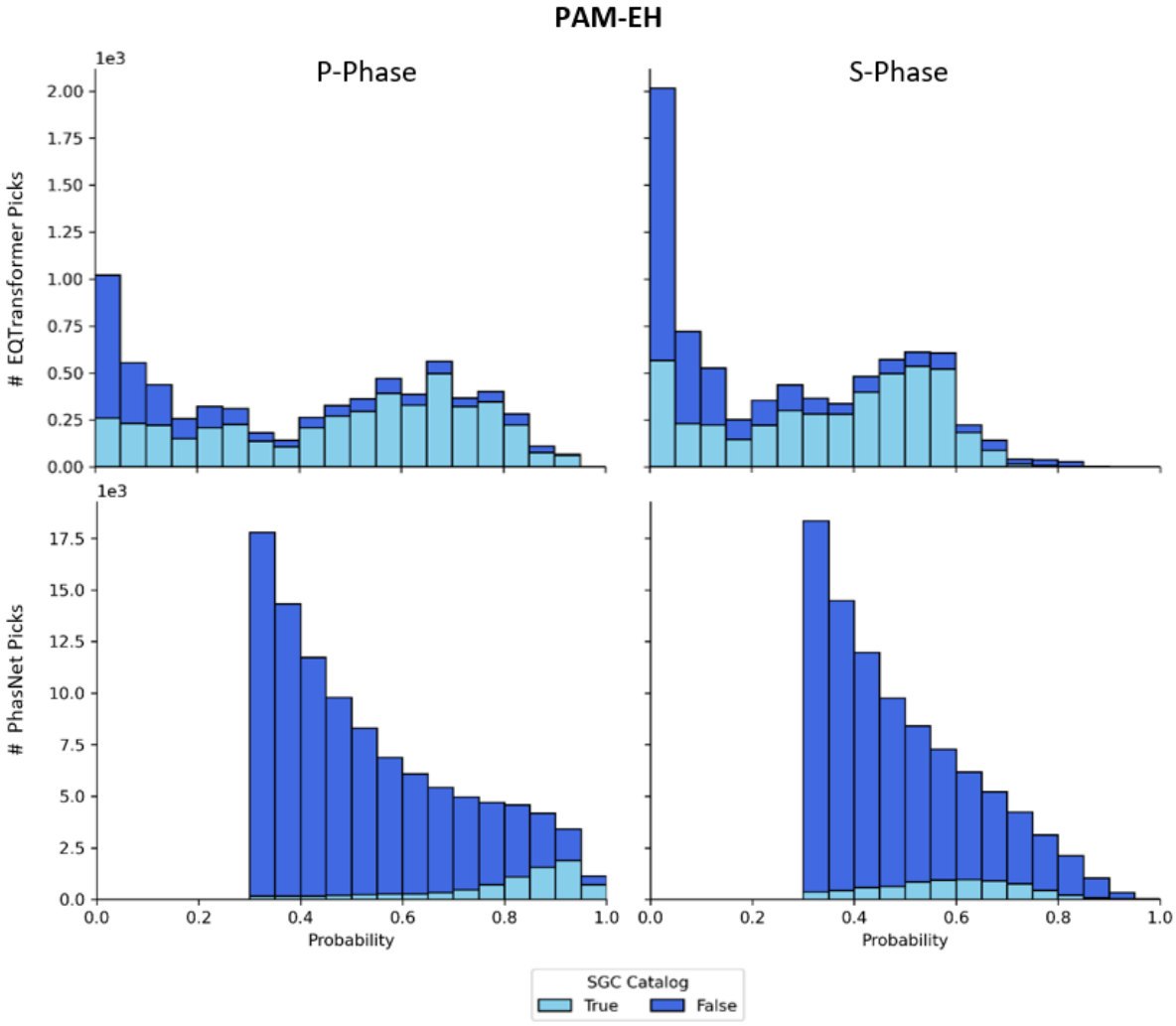

Figure 3-6: Stacked number of P and S picks as function of EQTransformer and PhaseNet probabilities for PAM station (EH instrument). The light blue bar represents the number of picks that were found in the SGC database. While the dark blue bar represents those that were not found.

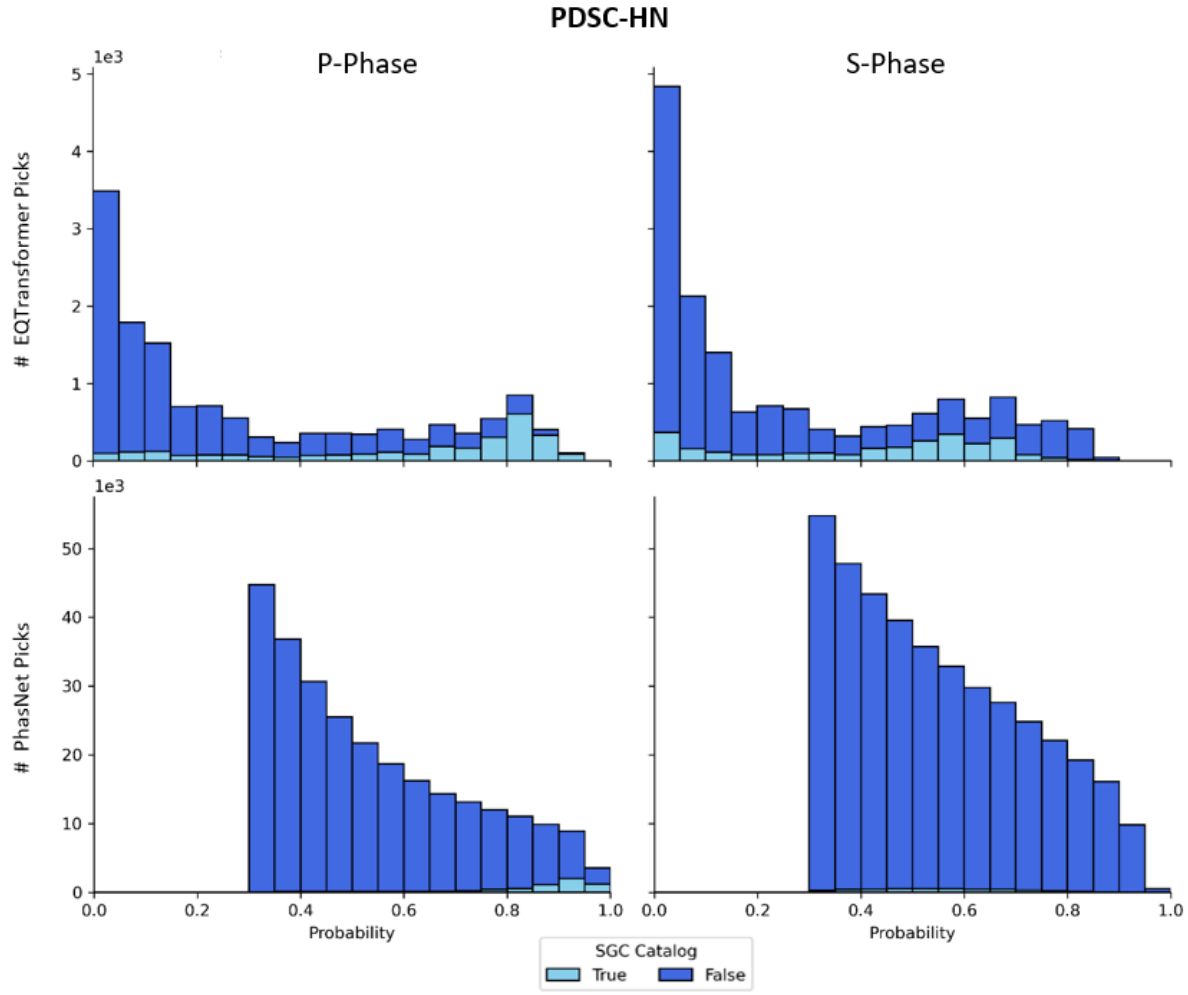

Figure 3-7: Stacked number of P and S picks as function of EQTransformer and PhaseNet probabilities for PDSC (HN instrument). The light blue bar represents the number of picks that were found in the SGC database. While the dark blue bar represents those that were not found.

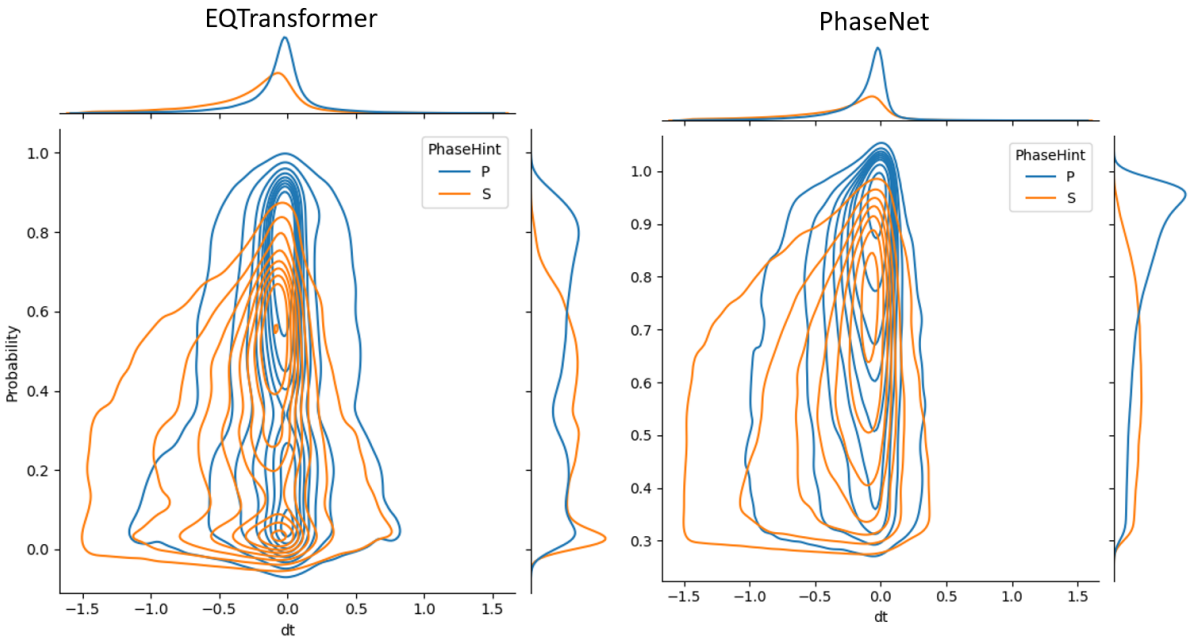

Figure 3-8: Comparison of the automatic time picks and manual picks of each seismic phase for both models. X-axis represents the time difference between picks (At most 1.5 seconds) and Y-axis represents the probabilities given by each model

To conclude, although PhaseNet performs better abilities to detect small earthquakes, EQTransformer provides more confidence in detecting true P and S phases. The scale of EQTransformer's number of picks is similar to that reported by the SGC, while PhaseNet overflows. On the other hand, since EQTransformer shows so many true picks at low probabilities, then it allows to have more confidence for results with high probabilities. This hypothesis is not necessarily true in PhaseNet because it sometimes assigns high probabilities to signals from external noises (usually where there are large amplitude changes). Finally, considering that the pre-processing for HH and EH instruments were the same in both models, the EQTransformer results suggest better performance on several types of instruments. This allows its operability in seismic networks with a wide variety of sensors.

4 Phase Association, Event location and Magnitude estimation

The content of this chapter is based mainly on the association results and their performance in obtaining reliable seismic catalogs of both regional and local networks. For the regional case we study the association performance for both PhaseNet and EQTransformer pickers in the CM seismic network. Association algorithms based on relocation procedures are very sensitive to false picks and clusters of picks that do not converge to an optimal location result. Therefore, we design an empirical filter for PhaseNet picks with the aim of obtain as many picks associations as possible without losing too many pick detections. As the EQTransformer picks are more reliable, this intermediate step was not necessary. Lastly, we compare the seismic catalogs and the magnitude estimation obtained from PhaseNet and EQTransformer picks with the manual catalog and other automatic catalogs.
From the regional results, we decided to use only EQTransformer for the VMM and YU local seismic networks, where we observed, association algorithms based on relocation procedures perform much better than the regional case, and therefore, the quality and operability of the EQTransformer results can be exploited much more.

4.1 Regional networks

For the regional case we study the association performance for both PhaseNet and EQTransformer pickers in the CM seismic network. The Scanloc module from SeisComP3 was used to associate those picks. It determines hypocenter solutions using cluster search and relocation procedure. We used LOCSAT and HYPO71 locator methods together with the velocity models IASPEI91 and Colombian 1D velocity model [Ojeda and Havskov, 2001], respectively, as inputs to the relocations performed in Scanloc. Therefore, we got seismic origins by each method. This was done because some picks were discarded by one locator because did not achieve a good fit, while the other did. So we finally merge the origins and remove duplicates.

4.1.1 Association performance in the CM network

Subsection 3.2.2 suggests the need for a robust associator algorithm that apart from associating picks to different sources, it must also ignore false picks so as not to degrade the event location

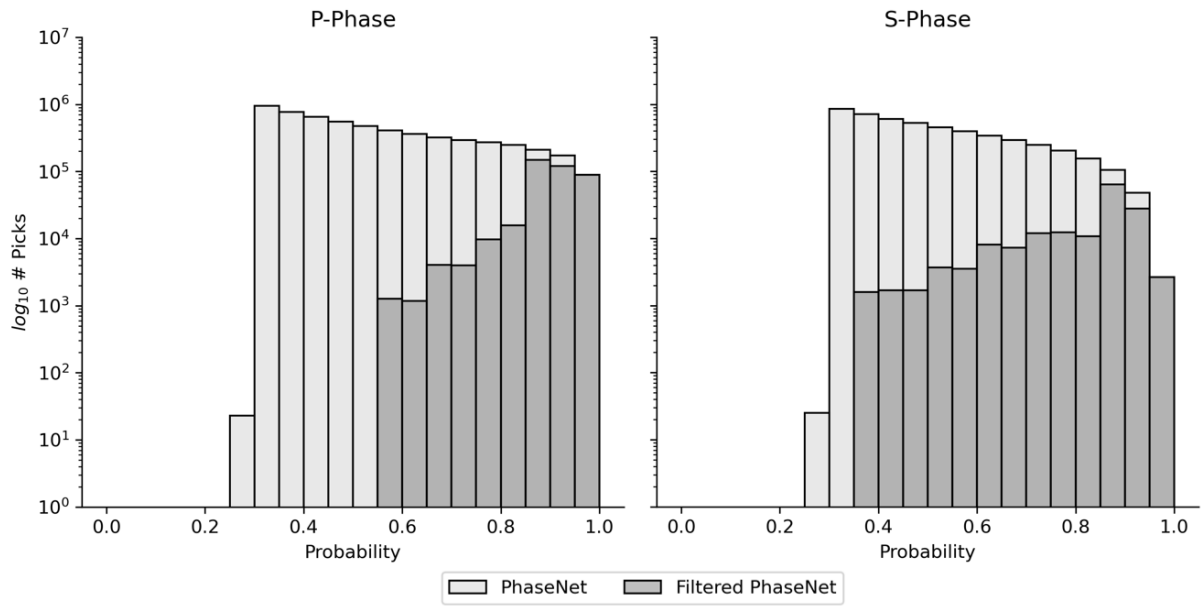

Figure 4-1: Number of filtered picks in PhaseNet.

accuracy, an important issue to address for PhaseNet in particular.

The first attempt to associate PhaseNet picks failed because we were considering the full range of the picks probabilities, and several of them were false picks. Therefore, we explore filters to clean the pick database. In the subsection 3.2.2, we also approached the probability analysis and we found true picks if the time difference between PhaseNet and SGC pick is less than 1.5 seconds. We filter PhaseNet picks by each station and based on the lowest probability bin that meets the following condition:

$$3T_p \geq F_P \tag{4-1}$$

where T_p and F_P represents the quantity of true and false picks respectively. For example, in the figure **3-5**, PhaseNet's P and S picks at station BAR2 were filtered since 0.8 and 0.6 probability values respectively. Sometimes this condition never was satisfied as PhaseNet results in the figure **3-7**. In these cases, we filter them from probability values of 0.85 for HH and EH instruments, and 0.95 for HN.

Figure **4-1** shows that the filter allows us to eliminate a large number of picks in PhaseNet. We chose the filter condition considering several tests in one week of data. The test aimed to find the right probabilities for each station, so that the picks could be associated, but not too strict to loose too many earthquakes.

However, the choice of an optimal filter is a very difficult task because there are several false picks with high probabilities, and several true picks with low probabilities.

Figure **4-2**-a represents an example of PhaseNet associations in two hours of seismic aftershocks in the CM network. The filter reduced a lot of picks to be able to associate the remaining ones. Although most of the false picks were eliminated, many of the real ones were also removed.

Then, we were able to obtain some associations with a small number of phases. Thus, the filter allows to have event detections but it substantially decreases the quality.

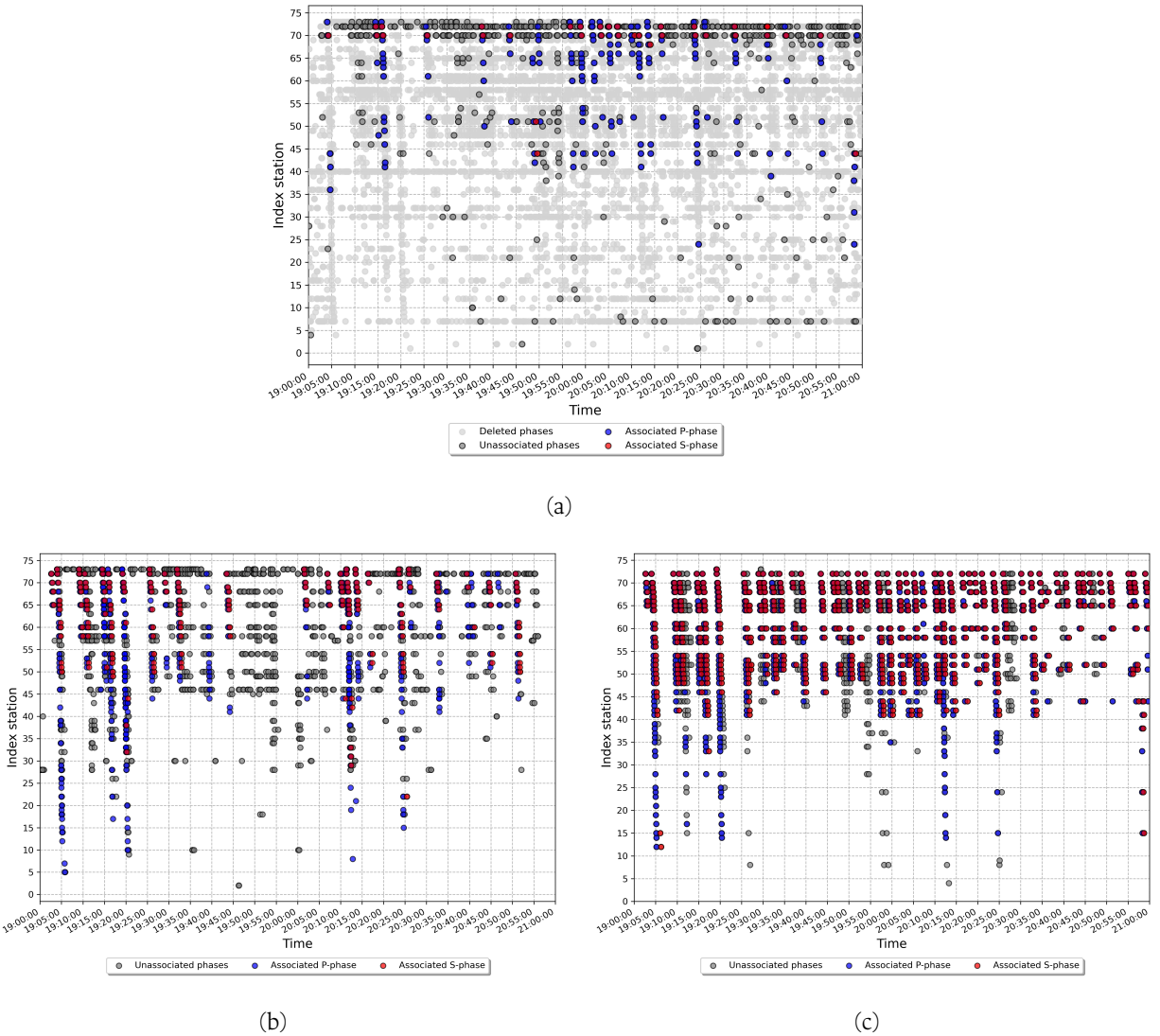

Figure 4-2: Associated phases by picker in two hours of seismic aftershocks. Station indices are sorted so that the last index corresponds to the station closest to the epicenter of the main earthquake at 19:03 UTC. a) PhaseNet. b) EQTransformer c) Manual SGC picks

As EQTransformer outputs have more confidence, the Scanloc module was able to associate more picks (Figure **4-2**-b). Even for picks manually verified almost all picks were associated (Figure **4-2**-c). This can be seen in the association statistics of both models for all picks obtained for the CM network (Figures **4-3**-a & **4-3**-b). The Scanloc module associates many more picks for EQTransformer than for PhaseNet. In addition, it is shown that more than eighty percent of the verified SGC picks were successfully associated for both P and S phases. While for both

PhaseNet and EQTransformer the association percentages were remarkably low for the entire range of probabilities. Therefore, there are much more rejected picks than associated picks.

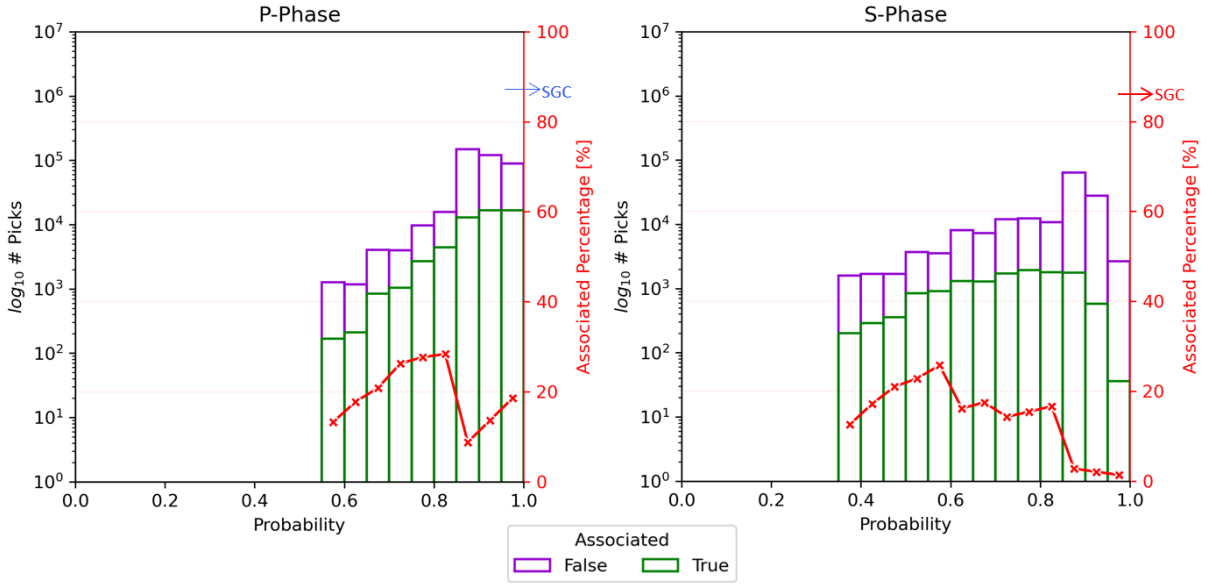

(a)

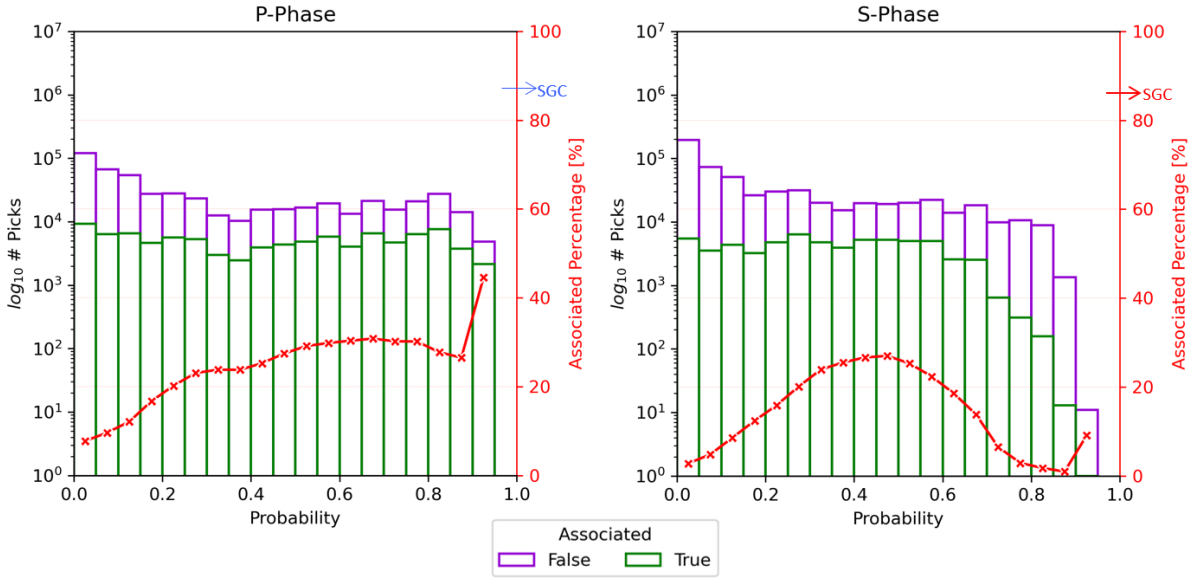

(b)

Figure 4-3: Associated and unassociated picks by picker in the CM seismic network. Left y-axis represents the amount of picks in logarithmic scale and the right y-axis shows the associated percentage of picks. The SGC label indicates the associated percentage of the total of SGC picks. a) PhaseNet b) EQTransformer

We note that the associator, in addition to being sensitive to false picks, also rejects true prelim-

inary associations whose locations do not converge. This happens because the appropriate picks are not associated or because there are not enough picks to converge to a solution. In turn, this can happen when there are too many picks; both positive or false, so close in time as to make it difficult to locate them. For that reason, association algorithms using location procedures can be a major bottleneck in the workflow to automatically detect events with DL models.
Finally, we show the number of associated picks provided by DL models that are not in the SGC catalog. In the case of PhaseNet, due to the filter used, most of the picks are found in the SGC catalog (Figure **4-4**-a). While, EQTransformer uses a notable amount of picks did not find in the SGC catalog (Figure **4-4**-b). Thus, EQTransformer complements the SGC database. Nevertheless, most of the associated picks are also in the SGC Catalog. Which, in turn, provides a degree of reliability.

4.1.2 Performance of the seismic catalog in the CM network

For each of the associations there is a preferred hypocentral location, thus, for each of the automatic pickers we obtain a seismological catalog. To obtain reliable locations we require for each earthquake at least:

- Minimum 4 P-phases and 2 S-phases per event.
- Uncertainties in epicentral location: $latitude \leq 15km$ and $longitude \leq 15km$
- Uncertainty in $depth \leq 30km$
- $rms \leq 2$

We calculate the moment magnitude M_w derived from m_B magnitude, and we compare the magnitude values with the manual catalog for the CM network. To compare, we join the events in the automatic and manual catalogs if each of them have similar origin time and come from the same source location. The origin time difference must be $\leq 1.5s$. The difference in the epicenter location must be $\leq 15km$ in latitude and longitude, and the depth difference must be $\leq 30km$. The picks recorded by each DL model allow the calculation of a magnitude consistent with the magnitude calculated from the manual picks (Figure **4-5**). Notice that the magnitude variance decreases as the magnitude increases.
Figure **4-6** shows the number of events per magnitude bin in the various catalogs obtained by each picker. SGC-manual are the phases picked and associated by the analysts, while SGC-auto are those picked by the analysts but associated by the Scanloc module. The first immediate result is that the automatic pickers are severely affected by the association algorithm, while Scanloc module works quite well to associate manual picks. Keep in mind that the manual catalog allows the analyst to move the pick given an initial guess, so taht if the association module wants to throw out a pick, the analyst can move it in order to keep it.

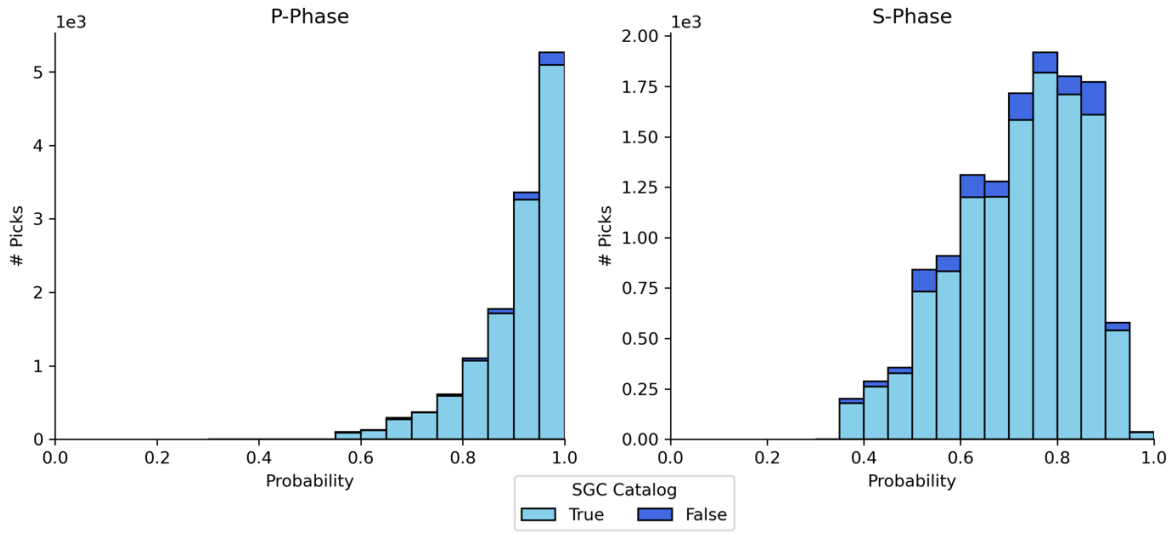

(a)

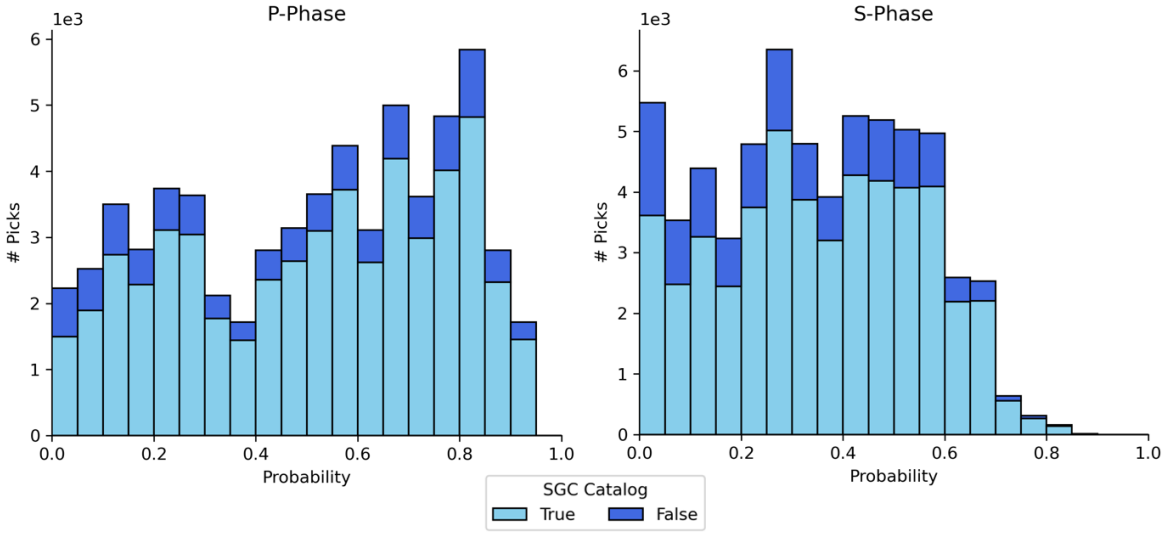

(b)

Figure 4-4: Stacked number of P and S associated picks as function of EQTransformer and PhaseNet probabilities. The light blue bar represents the number of picks that were found in the SGC database. While the dark blue bar represents those that were not found. a) PhaseNet. b) EQTransformer.

Nevertheless, it seems fair to compare the number of events obtained by each automatic picker. Despite having substantially filtered PhaseNet's picks, its results yield many more small events than the STA/LTA algorithm. Nonetheless, EQTransformer have the greatest number of events between them.

In conclusion both PhaseNet and EQTransformer pickers significantly improve the automatic

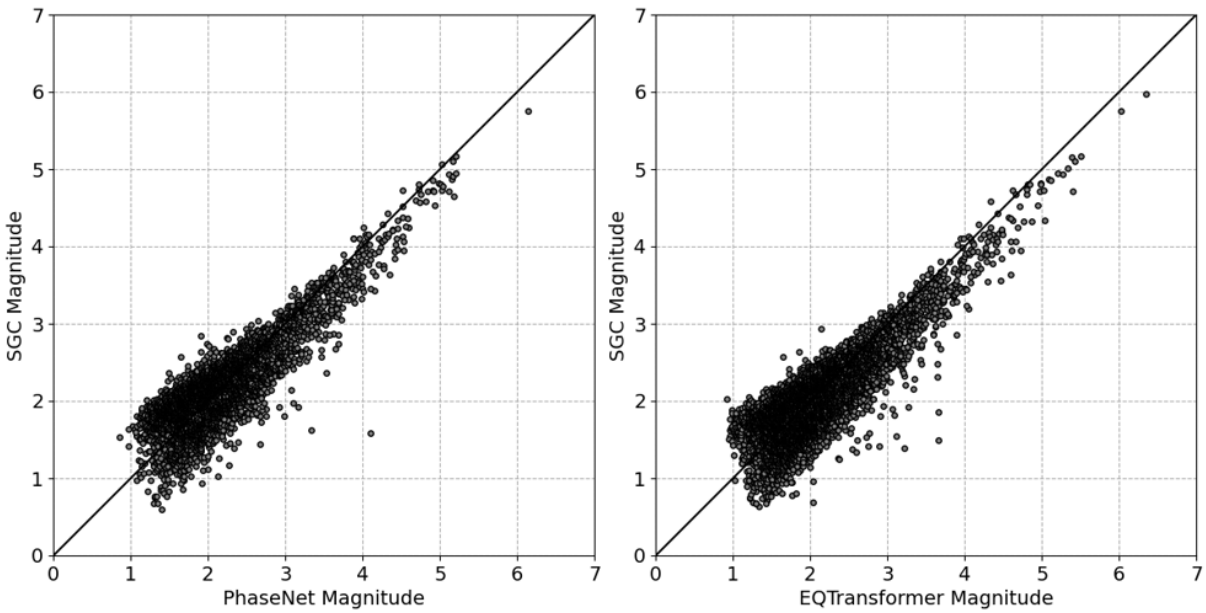

Figure 4-5: Comparison of the magnitude values calculated from the picks obtained by PhaseNet and EQTransformer versus those calculated manually by the SGC picks.

processing of the SGC. Even better, considering what we have seen in the analysis of the picks, they could complement or even exceed the manual results if there was a good associator for these types of picks.

4.2 Local networks

In agreement with the conclusions of chapter 3 and what was seen for the CM network, the EQTransformer picks were shown here optimal results for obtaining a high quality catalog. Therefore, we decided to only use EQTransformer for the VMM and YU local networks.
As for the association algorithm, we used the same association procedure for the VMM network as for the regional network. While for the YU network, for data privacy terms, we used the free association algorithm proposed in the EQTransformer repository. Unlike Scanloc, it links the phases based on detection times only. We used HYPOCENTER with the Colombian 1D velocity model to locate the seismic events. For this thesis, we have not calculated the magnitudes of the YU network events.

4.2.1 Association performance in the VMM and YU networks

As expected, the association algorithms work much better for local networks, and therefore, a significant gain is obtained from the small detections given by SDL models. In the VMM network the association percentage of the EQTransformer picks increase twenty percent more than in the

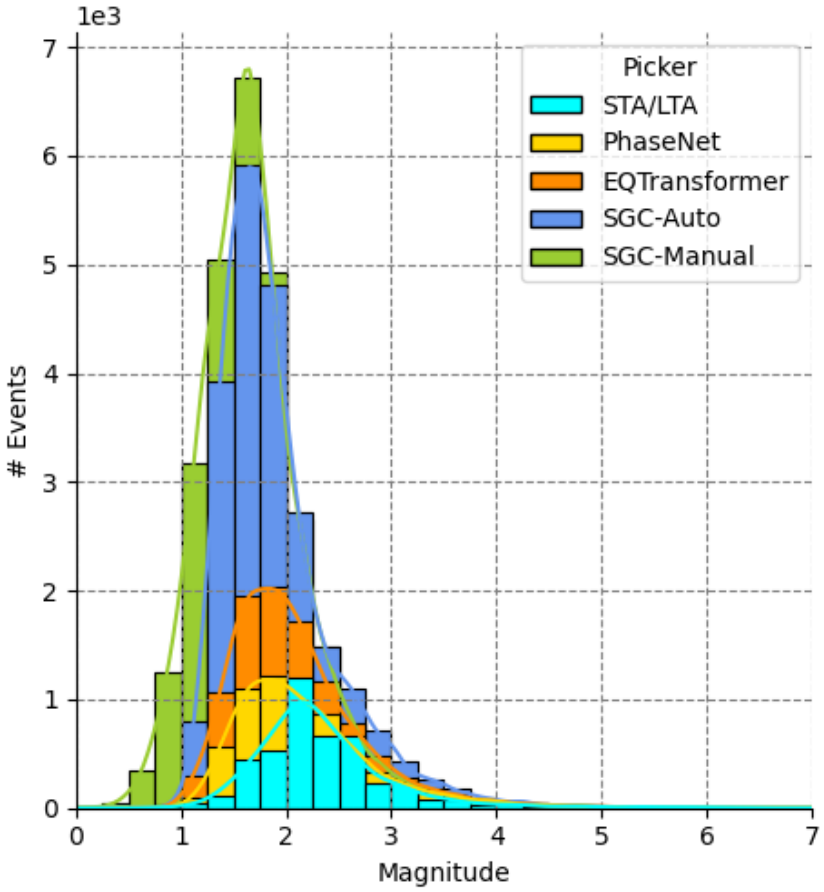

Figure 4-6: Number of events per magnitude by each picker in the CM network. SGC-manual are picked and associated by the analysts. The others are associated with the Scanloc module.

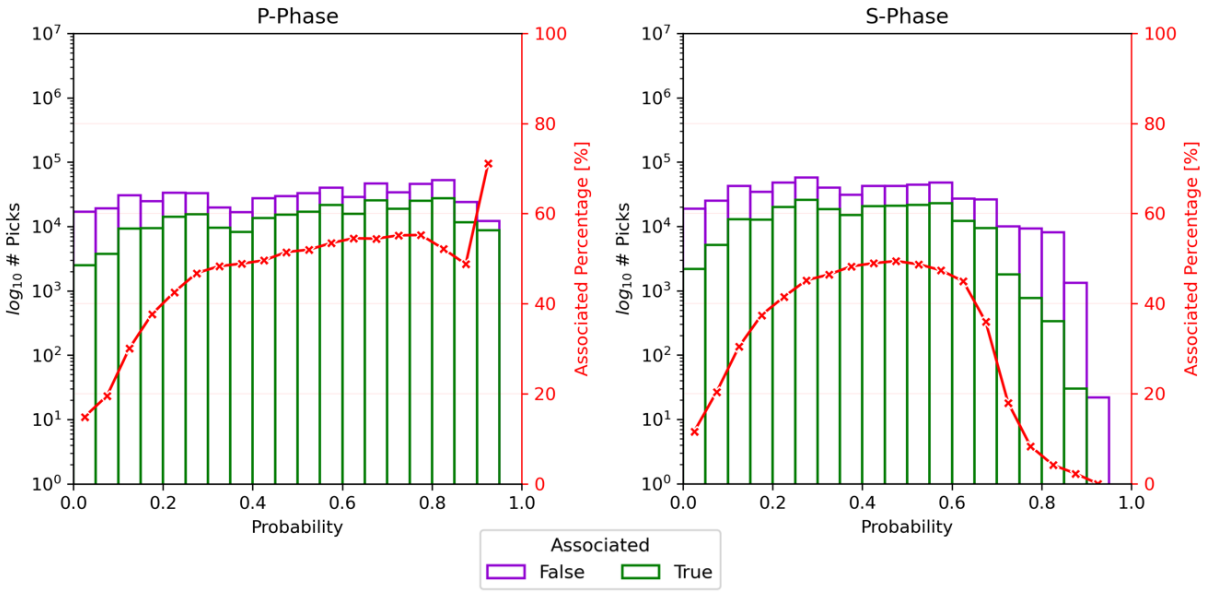

Figure 4-7: Associated and unassociated picks picked by EQTransformer in the VMM seismic network. Left y-axis represents the amount of picks in logarithmic scale and the right y-axis shows the associated percentage of picks.

CM network (Figure **4-7**). In local networks, Scanloc is less likely to reject picks because it is easier for associations to converge to a good solution.
On the other hand, we observe for both CM and VMM networks the same distributions of the percentage of association as a function of probability. For P-phases, the associated percentage increases as the probability increases. While for S-phases, it increases until 0.5 of probability and for higher probabilities it decreases. This is one of the weaknesses of associating by relocation. In this case, the S phases that are highly reliable could not be associated because it increased the rms of the trial location, or simply because the reference P-phase is not associated. Since the high probabilities in EQTransformer are so reliable, in these cases the problem may be due to the velocity model, since it cannot relocate with new S-phases.
We use the association algorithm proposed in the EQTransformer repository in the YU network results. In figure **4-8**, we can observe that the percentage of association remains at forty percent for all probabilities in both phases. When comparing the two local networks VMM and YU, we note that for phase P, the Scanloc module associates a higher percentage of picks. However, for S-phases, the association percentage is much higher in the algorithm proposed by EQTransformer.

4.2.2 Performance of the seismic catalog in the VMM network

The quality of the local catalog locations follows the same condition as in the regional network. In addition, we also calculate the moment magnitude M_w for the VMM network, and not for the

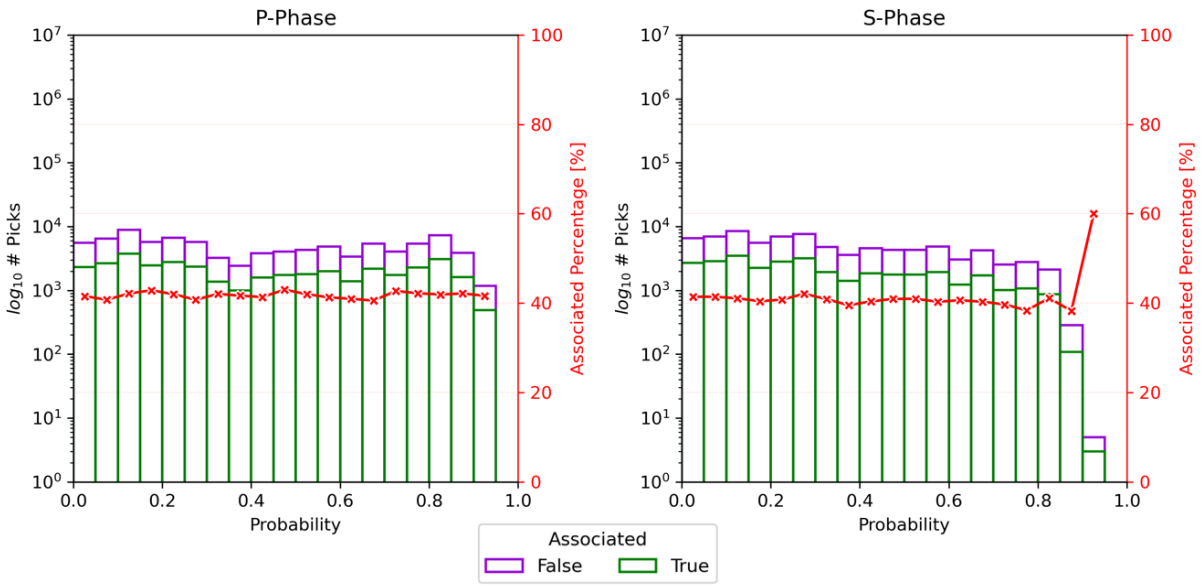

Figure 4-8: Associated and unassociated phases by EQTransformer in the YU seismic network. Left y-axis represents the amount of picks in logarithmic scale and the right y-axis shows the associated percentage of picks.

YU network.

Figure **4-9** show us the number of events per magnitude, showing that the detection ability was significantly improved. Events with lower magnitude than in the regional case are detected and located. This guarantees the ability of EQTransformer to detect small events with great reliability.

We compare the results with two SGC catalogs obtained from the seismic processing of the VMM network stations. Both report events with depth $\leq 50km$ and occurring within the VMM polygon (**2-1**). Both catalogs come from different working groups, therefore they are obtained with different velocity models and location methods.

The first catalog is the general baseline of seismicity (LBG) and the second is the TECTO catalog [1]. It should be clarified that the information contained in the LBG catalog is dynamic until the start of exploration activities. This dynamic behavior is due to the daily recording and reprocessing of new events in the VMM region.

Figure **4-10** shows that the LBG catalog is processed from the 2018 onwards, and the TECTO catalog did not report seismic events in June and December 2017. In both catalogs, there are 20 to 40 additional events per month compared with EQTransformer, and most of them have a magnitude less than 1. However, for magnitudes larger than 1, EQTransformer is able to detect additional ones as well, and therefore, may complement the manual database.

The magnitude of the events that are both in the SGC catalogs were compared with the magnitude of the catalog reported with EQTransformer. Figure **4-11** shows that the magnitude of the

[1]SGC Catalogs: `http://bdrsnc.sgc.gov.co/paginas1/catalogo/index.php`

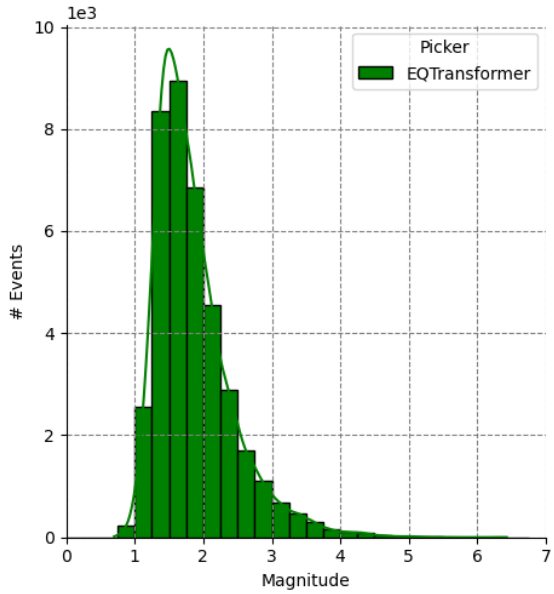

Figure 4-9: Number of events per magnitude picked by EQTransformer in the VMM network.

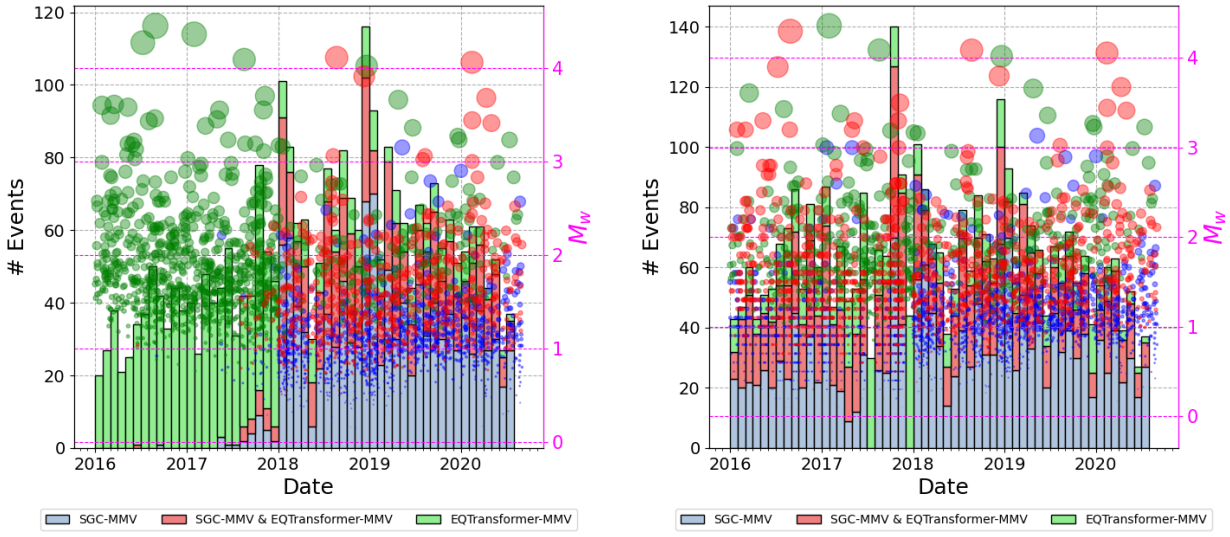

(a) (b)

Figure 4-10: Stacked number of events (depth $\leq 50km$) as function of time in the VMM polygon. a) Comparison with the LBG catalog. b) Comparison with the TECTO catalog.

automatic catalog is overestimated with respect to what is reported by both manual catalogs. We are not sure about the reason for this, but it is something to look at in future research.

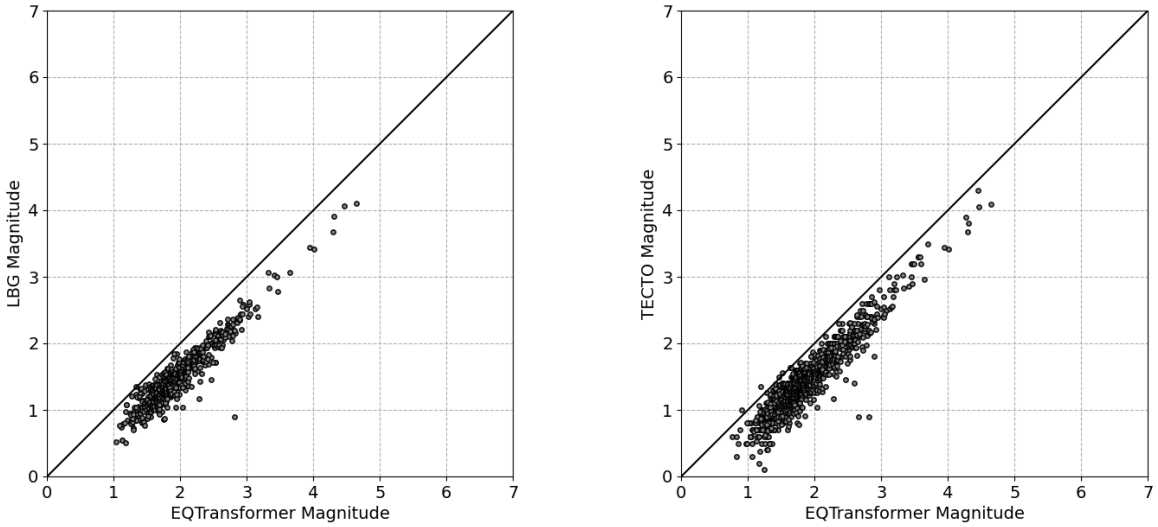

(a) (b)

Figure 4-11: Comparison of the magnitude values calculated from the picks obtained by EQ-Transformer versus those calculated manually by the SGC picks in the LBG and TECTO catalogs. a) Comparison with the LBG catalog. b) Comparison with the TECTO catalog.

5 Seismological catalogs

Seismological catalogs allow us to understand much of the physics of earthquakes, their relationship to active tectonics and individual faults, as well as the seismic hazard of a particular region. The resolution of the catalog depends on many factors, including the geometry of the seismological network, the instrumentation, and finally, the data processing performed. In this chapter we show the automatic seismological catalog obtained for the three seismic networks. In general, both PhaseNet and EQTransformer the automatic results for the national network are similar to the manual ones. And the results of the local networks show much better resolution in their respective region. We also show that each of the catalogs illuminate structures and fault systems that contribute to the knowledge of regional tectonics in northern South America. Finally, EQTransformer good performance as an autopicking algorithm and its compatibility with the association and location methods, inspired us to merge the catalogs in to one automatic seismic catalog to improve the visualization of the seismicity.

5.1 Catalogs obtained by each network

5.1.1 CM network

Figures **5-1**-a and **5-1**-b show the manual catalog reported by the SGC with the CM network. This catalog was developed mainly with the NonLinLoc locator [Lomax et al., 2000]. Unlike linear methodologies, it is a non-linear probabilistic earthquake locator, and, although it works slower, is better at giving an accurate image of seismic locations. For this reason, we do not expect to improve the manual locations, but we do expect to illuminate lineaments that allow us to define some faults and some tectonic structures.

The SGC catalog reflects the activity in the colombian territory. The seismic activity illuminates the major subduction processes due to the relative convergence between the Nazca, Caribbean and South American plates (Figure **5-1**-a) . In addition, there is also shallow seismicity along the various active fault systems (Figure **5-1**-b). This catalog highlights the main fault systems: The Llanos Foothill Fault System, the Magdalena Valley Fault System and the Romeral Fault (Figure **5-1**-c).

Both PhaseNet and EQTransformer catalogs are sufficient reliable to show asimilar distribution of intermediate seismicity in the Colombian territory (figures **5-2** and **5-3**). Furthermore, both also show the abrupt change in position of the Benioff zone in the Nazca plate around $5.5°$N

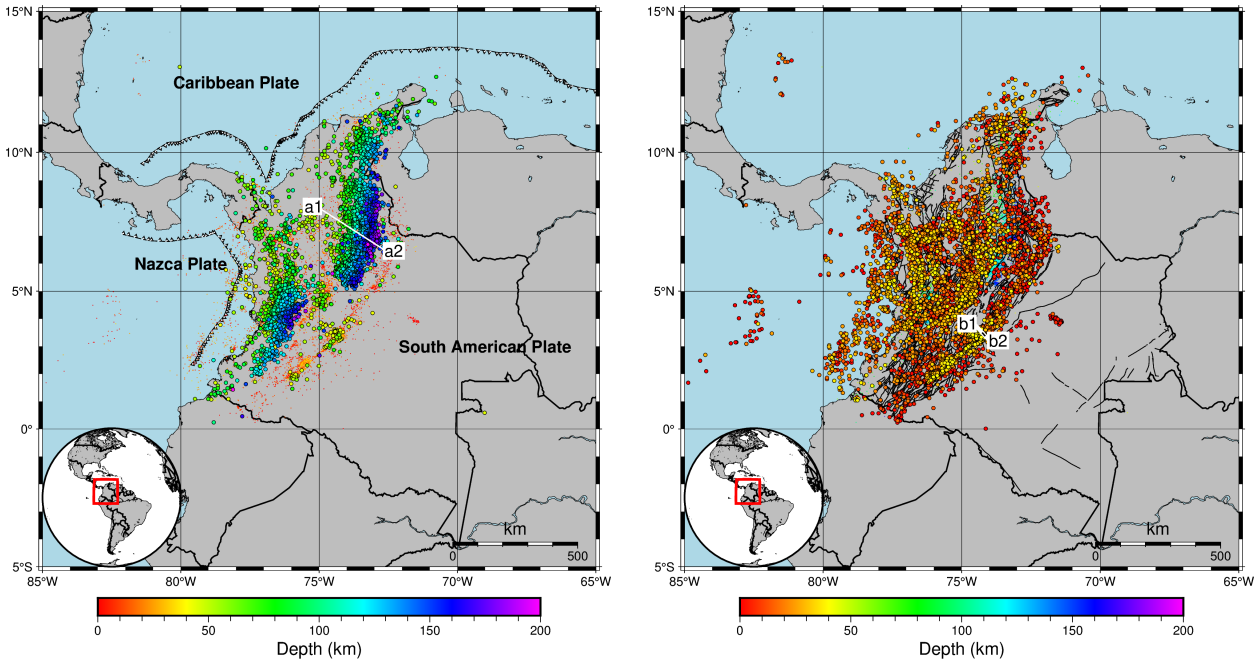

(a) Depths >= 40 km are highlighted

(b) Depths < 40 km are highlighted

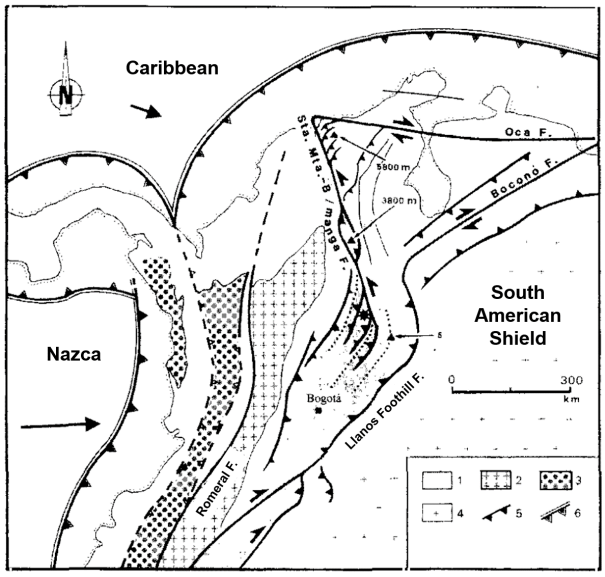

(c) 1. East Cordillera. 2. Central Cordillera. 3. West (oceanic affinity). 4. Craton. 5. Thrust and reverse faults. 6. Subduction zones

Figure 5-1: a-b) SGC Manual catalog using the CM network. c) General tectonic framework of the Northern Andes. Taken from [Fuenzalida et al., 1998]

[Ojeda and Havskov, 2001, Vargas and Mann, 2013, Syracuse et al., 2016, Sun et al., 2022]. At the same latitude, volcanic activity also ceases at 5 Ma [Wagner et al., 2017, Kellogg et al., 2019].

These evidences have generated multiple geoscientific debates. On the one hand, they have been interpreted as a tear in the Nazca plate [Vargas and Mann, 2013, Syracuse et al., 2016]. Where two subduction styles are generated [Chiarabba et al., 2016], a normal subduction with associated volcanic arc towards the south and a flat subduction without volcanism to the north. On the other hand, they are interpreted as the expression of two subduction processes [Fuenzalida et al., 1998, Sun et al., 2022]. Where intermediate seismicity from $5°N$ to the south is associated with a diacronic ocean-continent subduction process [Martinez, 2016]; generating insufficient conditions to generate dehydration of the lithosphere in subduction, and intermediate seismicity between $5°N$ and $8°N$ under the Cordillera Oriental is explained as a complex continent-continent subduction process [Syracuse et al., 2016, Sun et al., 2022]. Previous authors refer to the northern slab as Bucaramanga segment and the southern slab as the Cauca segment. In this work we use this convention.

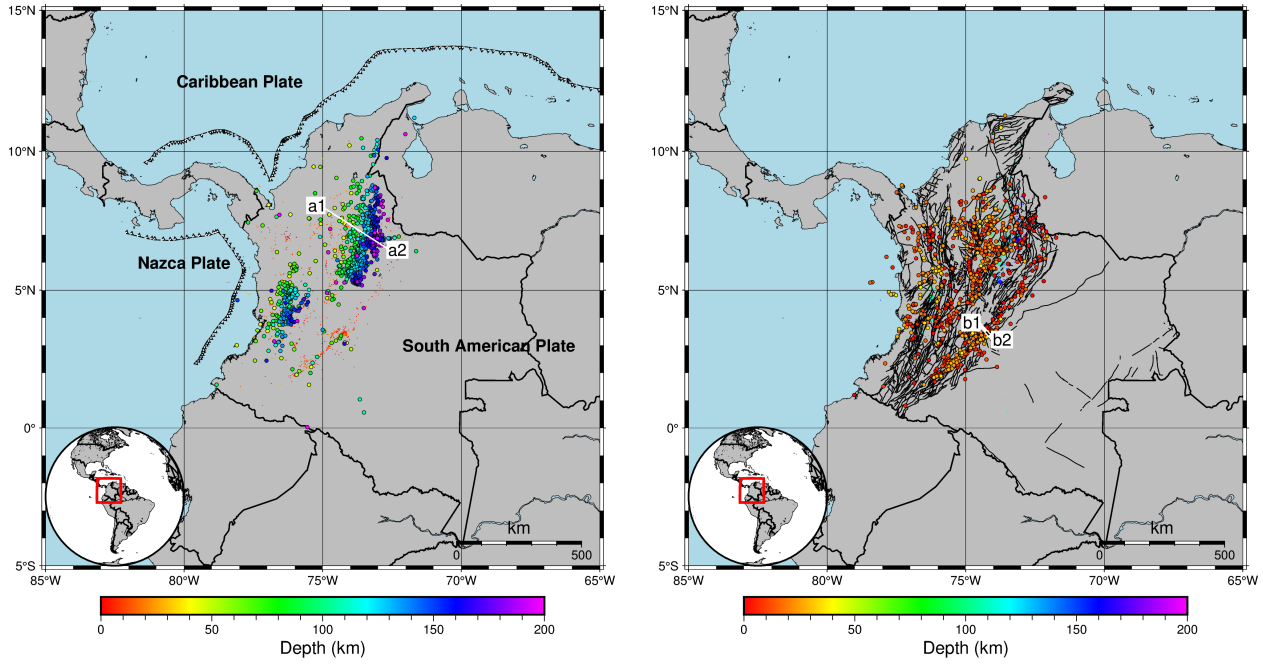

(a) Depths >= 40 km are highlighted

(b) Depths < 40 km are highlighted

Figure 5-2: PhaseNet catalog using the CM network.

Figure **5-4** shows the same seismic profile a1-a2 for the three catalogs but with different widths in the Bucaramanga segment. Both seek to contrast the quality of the catalogs in this zone. The first transect only has a total width of $10km$ to mainly illuminate the Bucaramanga nest (figure **5-4**-b). While the second is $100km$ wide to delineate the Benioff zone associated with the Nazca subduction (figure **5-4**-c). Both automatic catalogs allow to recognize the same location of the volume associated with the Bucaramanga nest. It has an elliptical shape elongating in down-slip direction [Zarifi et al., 2007]. Our results suggest that the nest is centered at $6.875°N$ and $73.115°W$ at 150 km approximately. Likewise, both catalogs depict the subduction in the

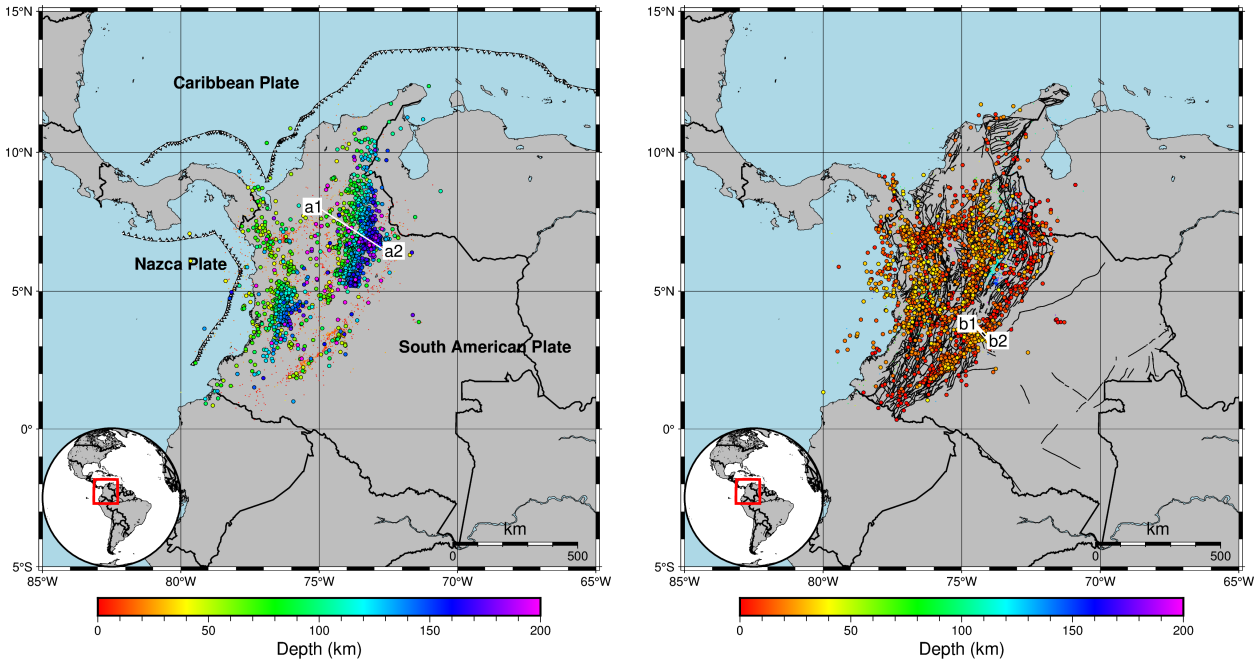

(a) Depths >= 40 km are highlighted

(b) Depths < 40 km are highlighted

Figure 5-3: EQTransformer catalog using the CM network.

Bucaramanga segment.

In all catalogs there is a change in the direction of the deepest seismicity precisely at the location of the Bucaramanga nest [Sun et al., 2022]. The northern part of the segment has a strike of $\sim N10°E$ down to $7°N$, further south, the segment has a strike $\sim N35°E$.

EQTransformer show better results to draw the system of surface faults than PhaseNet. They are good enough to delineate the systems of Llanos foothill fault and Magdalena Valley. And only EQTransformer is able to illuminate seismicity in the Romeral fault (figures **5-3**-b and**5-1**-c). It also is able to locate some earthquakes induced by massive wastewater injection near Puerto Gaitán inside the quadrant: $[3.65, 4.05, -71.67, -71.23]$ [Molina et al., 2020]. We highlight the previous result because these earthquakes are difficult to locate with an automatic algorithm, mainly because of the large azimuthal GAP implied by the geometry of the stations (figure **2-1**), and also because the simple model of subsurface velocities does not allow it.

Figure **5-5**-a shows the seismic profile b1-b2 of the SGC manual catalog. The transect is only 5 km wide and illuminates a large volume of aftershocks generated by a M_w mainshock in Mesetas-Meta at a depth of 13 km. This set of aftershocks is located in the Algeciras fault and are located within the first 20 km depth [Mayorga et al., 2020]. PhaseNet and EQTransformer catalogs also detect a large number of events in the transect (figures **5-5**-b and **5-5**-c). However, both show the lineament only in the first 5 km depth due to the limitations of the location algorithms.

The automatic catalogs used the LOCSAT and HYPO71 location algorithms, while the manual used NonLinLoc. We compared the aftershock locations in the c1-c2 profile with the same 5 km

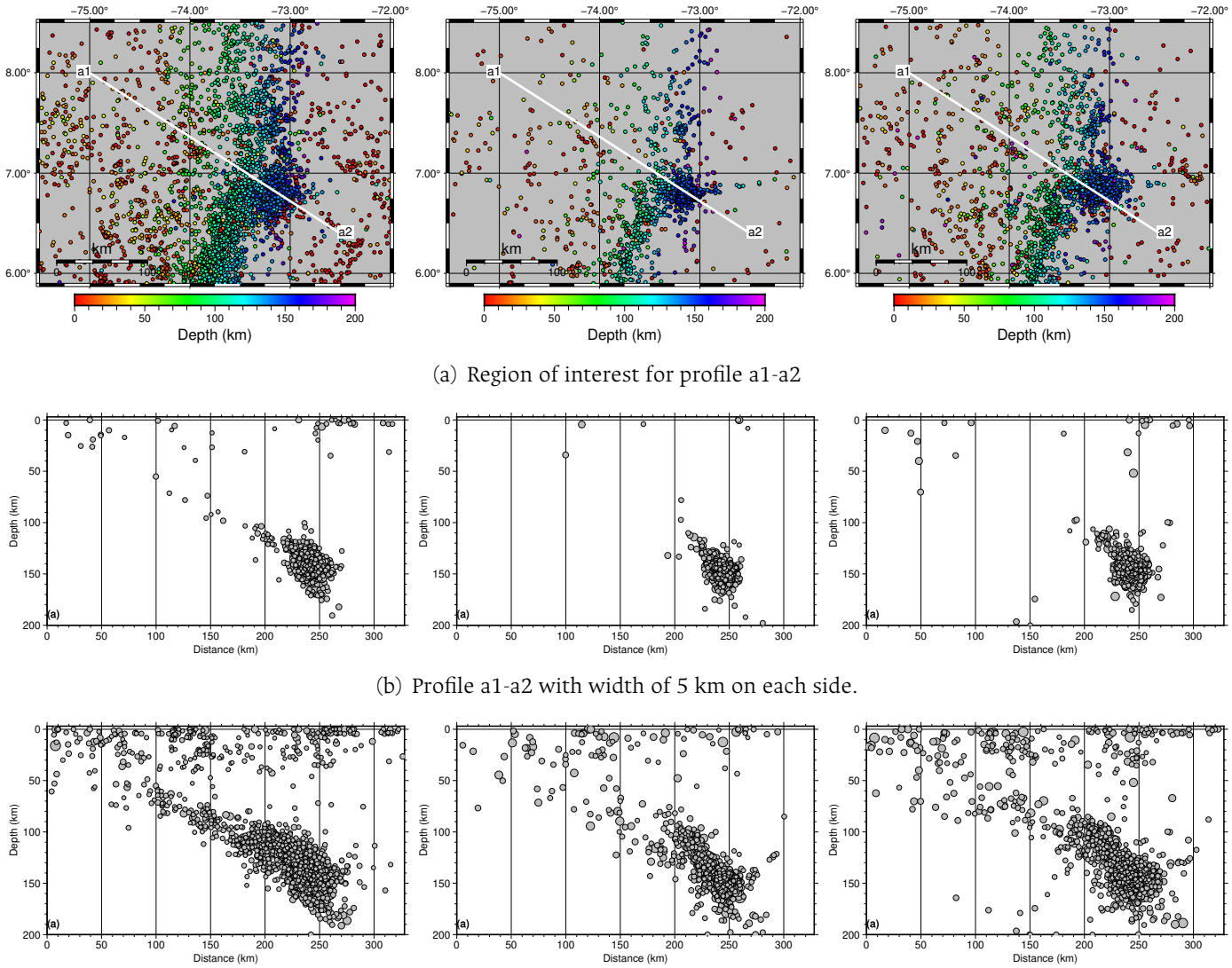

(a) Region of interest for profile a1-a2

(b) Profile a1-a2 with width of 5 km on each side.

(c) Profile a1-a2 with width of 50 km on each side.

Figure 5-4: a1-a2 profile using the CM network. From left to right column: Manual, PhaseNet and EQTransformer catalogs.

of width for the first two days after the mainshock (figure **5-6**). The SGC-manual catalog shows that the main event is located at a depth of 13 km, and the highest magnitude aftershock is close to it at a depth of 8 km (figure **5-6**-a). The rest of the aftershocks are located at the grid nodes where the NonLinLoc solution converges. It appears that the nodes are distributed every 1km, which limits the resolution of the locations. On the other hand, catalogs obtained from LOCSAT and HYPO71 show a different behavior (figures **5-6**-b-d). Basically, most of the events are fixed in the first 5km depth. This happens even for the SGC-auto catalog (figure **5-6**-d), which has almost the same as the manual catalog picks associations (figure **4-2**-c), and therefore, almost the same number of events (figure **4-6**). The main difference is that was located with the same

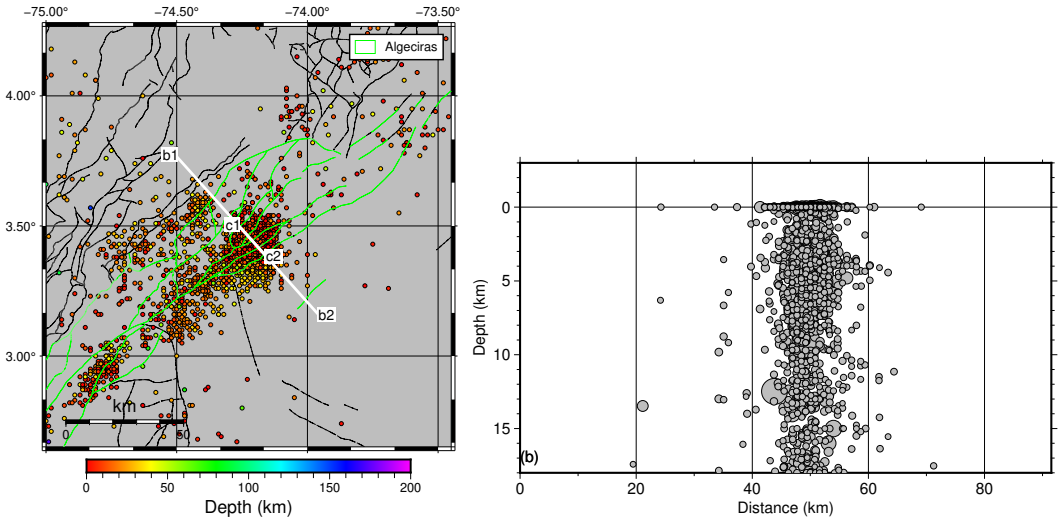

(a) On the left the region of interest for profiles b1-b2 and c1-c2. On the right the b1-b2 profile with the manual catalog.

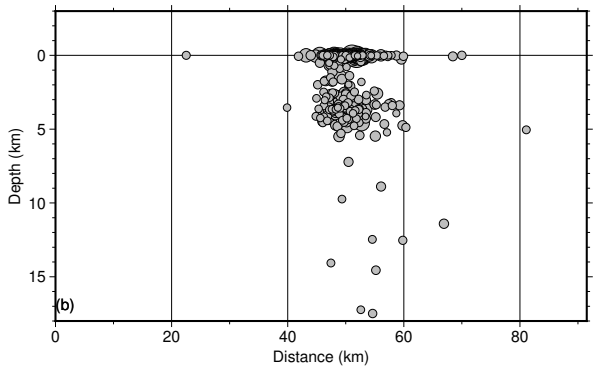

(b) b1-b2 profile using the PhaseNet catalog.

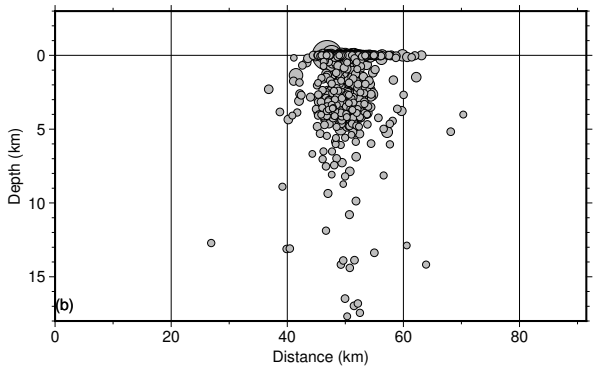

(c) b1-b2 profile using the EQTransformer catalog.

Figure 5-5: b1-b2 profile with width of 2.5 km on each side using the CM network.

location methodology as EQTransformer and PhaseNet. Therefore, the location algorithms used in this work allow us to illuminate structures and faults in a general way. If you want to study the detail, to the point of analyzing micro-faults, we recommend the use of more sophisticated location algorithms, including for example hypoDD [Waldhauser, 2001]. We did not attempt to do this, as it was beyond the scope of this work.

5.1.2 VMM network

Beyond human-induced monitoring purposes, the VMM network is also useful for a scientifically interesting region. It is located in a zone where three tectonic plates converge [Taboada et al., 2000, Cortés et al., 2005, Vargas and Mann, 2013, Syracuse et al., 2016, Wagner et al., 2017, Londoño et al., 2019, Londoño et al., 2020], and is contiguous to the Bucaramanga nest [Prieto

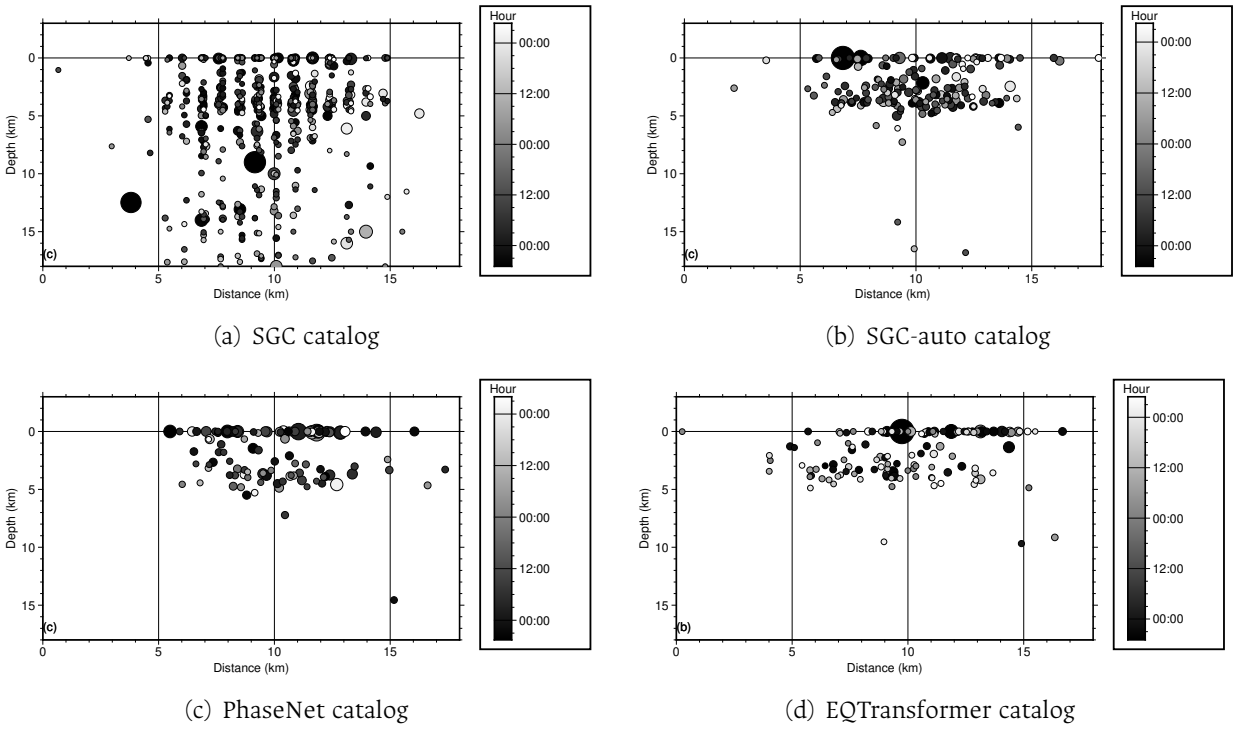

(a) SGC catalog

(b) SGC-auto catalog

(c) PhaseNet catalog

(d) EQTransformer catalog

Figure 5-6: c1-c2 profile with width of 2.5 km on each side using the CM network for the first two days after Mesetas-Meta main earthquake. The region of interest is shown on the map in figure **5-5**

et al., 2012, Zarifi et al., 2007]. Close to where we observed a sudden change in the strike direction in the subduction of the Bucaramanga segment. In addition, it is still unknown whether the Bucaramanga nest belongs to the Caribbean or Nazca Plates [Kellogg et al., 2019, Yarce et al., 2014]. Then, we hope to contribute to the state of the art from what we have observed in the VMM network catalog. It was obtained in a fully automatic way from the phases picked by EQTransformer. We also hope that our contributions will be of great motivation to encourage automatic monitoring based on deep learning.

The VMM network catalog is presented in figure **5-7**. The catalog results are much better than the CM network results. At first glance, the VMM network catalog is very similar to the manual catalog obtained in this region for the years 2014-2017 [Londoño et al., 2019]. Furthermore, the catalog is able to show in more detail the change in the strike direction in the subduction of the Bucaramanga segment. We estimated that the northern part of the segment has a strike of $\sim 5°$ and the southern has $\sim 28.32°$ .As we suggest, in the CM network, the Bucaramanga nest is the place where this change is taking place [Sun et al., 2022].

We draw some profiles to the see the geometry of the subducing slab (figure **5-7**-a). Previously, cross sections have been made for this region every $10°$ in azimuth for subduction earthquakes at VMM [Londoño et al., 2019]. In contrast, we decide to depict perpendicular profiles to the strike

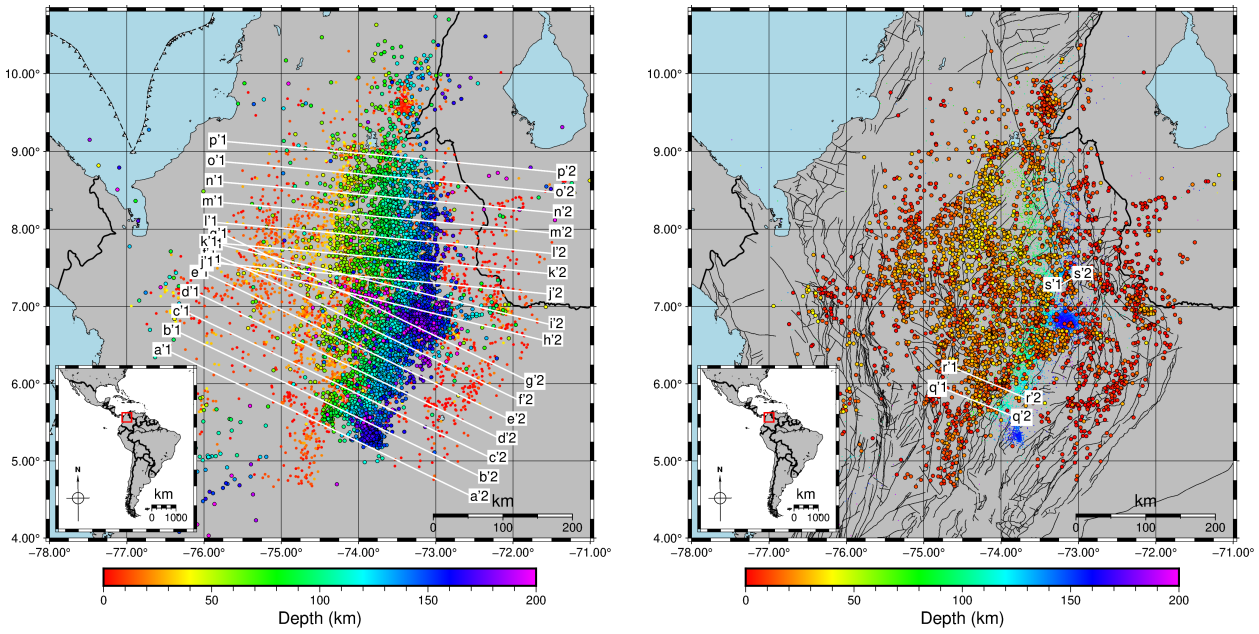

(a) Depths >= 40 km are highlighted

(b) Depths < 40 km are highlighted

Figure 5-7: VMM catalog.

direction. Figure **5-8** shows the evolution of the slab geometry of the Bucaramanga segment. In the profile a'1-a'2, the slab is illuminated to approximately 160 km depth and dipping at $\sim 50°$. b'1-b'2 shows a seismic cluster between 150 and 160 km deep, which projected on the surface is located at $5.31°N$ and $73.77°W$ close to the municipalities of Ubaté and Cucunubá. To date there is not much information about this seismic cluster. Further northeast, profiles g'1-g'2 and h'1-h'2 show the Bucaramanga nest at 150 km depth. In these profiles the slab dips as much as $55°$. In addition, greater depths, at distances 200-300 km of these profiles, a peculiar curvature not seen in any previous research is shown. It is in the opposite direction to the dip of the subducting slab. Besides, the profile i'1-i'2 shows a thin and strange alignment in the same direction as the curvature, but a few kilometers after the Bucaramanga nest, it curves more steeply until it reaches the surface. Finally, from j'1-j'2 to p'1-p'2, similar to previous results, the usual geometry of the Benioff zone is observed. At these heights it dips with an angle of $\sim 51.3°$.

We are not completely sure about the strange and funny folds we observed in g' to i' profiles because, after all, the catalog was processed automatically. Despite the careful filters we used, some events in the catalog could have escaped, and thus, generate misinterpretations. However, we show these results because the other results have shown full coherence with what has been studied to date, which gives us some confidence.

The VMM basin is limited to the northeast by the Santa Marta-Bucaramanga fault system, to the east and SE by the Salinas, Bituima and Cambao fault systems, and to the west by the Central Cordillera foothills [Pardo Trujillo, 2007, Londoño et al., 2019]. By studying the shallow seis-

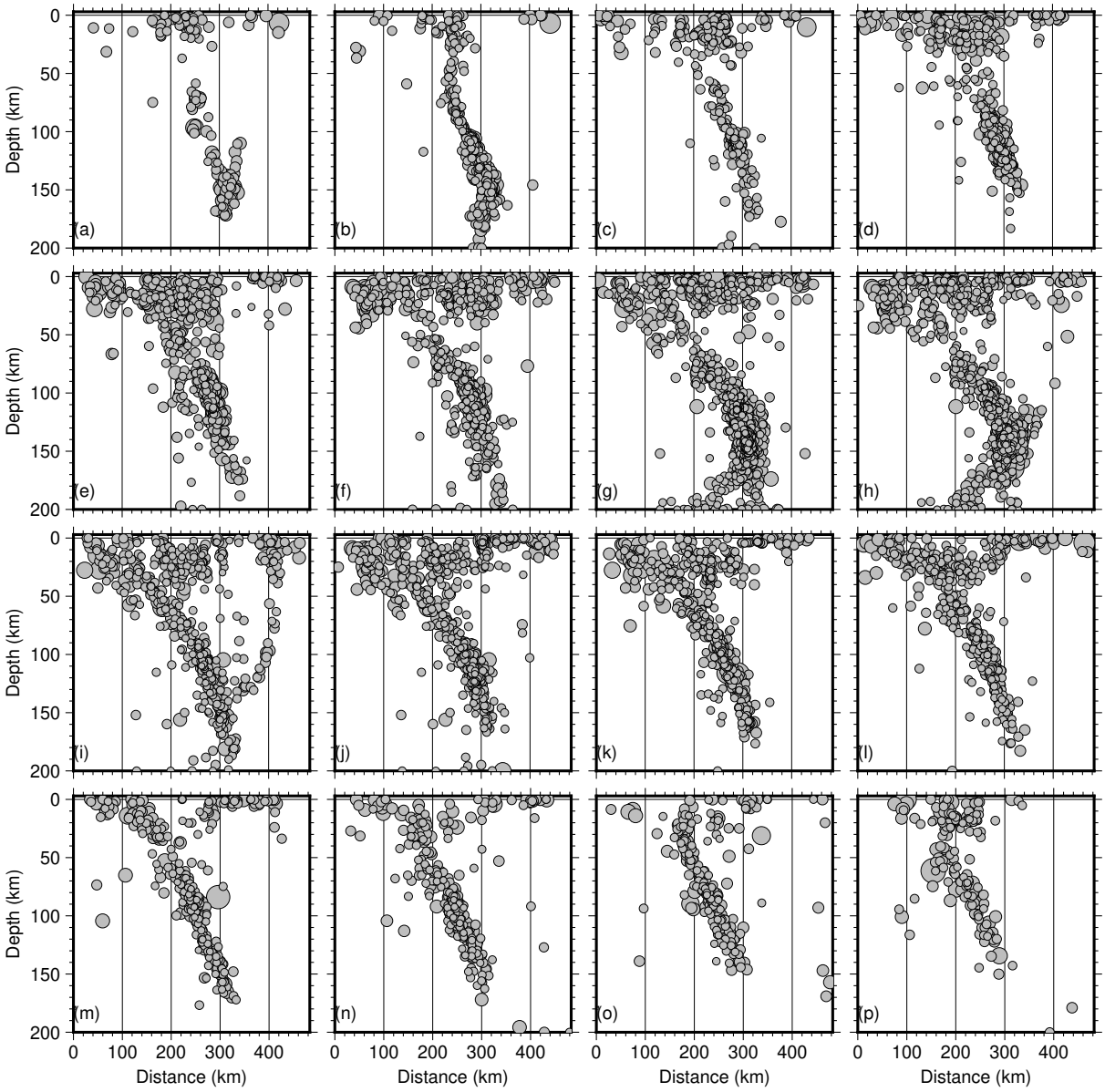

Figure 5-8: a' to p' profiles in the VMM catalog as shown in figure **5-7**-a. They are 15 km wide on each side. So the profiles do not intersect earthquakes between them.

micity, through some profiles, we illuminate seismicity associated with some of these systems of faults (figure **5-7**-b). Profiles q'1-q'2 and r'1-r'2 are drawn perpendicular to the strike of the La Salina fault system (**5-9**). This set of faults have an average strike $N30°E$ and moderate dip (30°ESE) [Taboada et al., 2000]. The profile q'1-q'2 shows seismicity in the first 30 km of depth, between 30 and 40 km away from the profile. Ít is associated to the La Salina Fault system. However, the profile r'1-r'2 shows two sectors of seismicity. The western sector is related with the Cambrás fault, it is characterized by being in a system of faults located in the middle zone of the VMM basin, mainly in a NS direction [Taboada et al., 2000]. While the eastern sector continues to illuminate the La Salina fault. Finally, in figure **5-10**, s'1-s'2 profile, we also illuminate a portion of seismicity that occurs parallel to the the Santa Marta-Bucaramanga fault, one of the major faults in northern Colombia bounded by the triangular Maracaibo block [Taboada et al., 2000, Londoño et al., 2019].

5.1.3 YU network

The lack of instrumentation in the northern zone of South America is one of the main reasons why the understanding of the Caribbean subducting plate has been limited. Besides, the complex tectonic setting also makes it flexible to multiple interpretations [Taboada et al., 2000, Vargas and Mann, 2013, Cortés et al., 2005, Sun et al., 2022, Cornthwaite et al., 2021]. Mainly based on regional seismic tomography models [Vargas and Mann, 2013, Chiarabba et al., 2016, Syracuse et al., 2016], local seismicity or on surface wave data. Recently, thanks to the YU network, it was possible to illuminate Caribbean subduction through finite frequency teleseismic P-wave tomography [Cornthwaite et al., 2021] suggesting it as a flat subduction. It was found that the northern limit of subduction lies south of the Oca-Ancón fault of northern Colombia and Venezuela. And although the southern boundary was not clearly defined, it was understood like a confluence of overlapping and confluence slabs. The YU network was also used to process teleseismic data in the CARMA region to produce a finite-frequency tomography model [Sun et al., 2022]. They found that there is an overlap between the Nazca and Caribbean subduction north of the "Caldas Tear". Furthermore, they claim that Bucaramanga nest occurs within the Caribbean plate. Although our objective is to present the resolution of the catalog obtained from the monitoring of the YU network, we also hope that our results will contribute to build ideas for the great tectonic debate in northwestern South America.

The YU catalog is presented in figure **5-11**. Even though the processing time of the YU network is much less than that of the VMM network, we observe that some interesting lineaments can be drawn for depths less than 40 km (figure **5-11**-b), and some areas of minining explosions were satisfactorily represented. On the other hand, the deep events were mainly located to the north (figure **5-11**-a).

We draw some profiles to get an idea of the geometry of the subduction and to represent some faults in the area (figure **5-11**). Figure **5-12** shows subduction zone, with profiles b" to f" clearly showing the Benioff Zone. In the profile d"1-d"2, we estimate the slab dip at 25°. Tomography

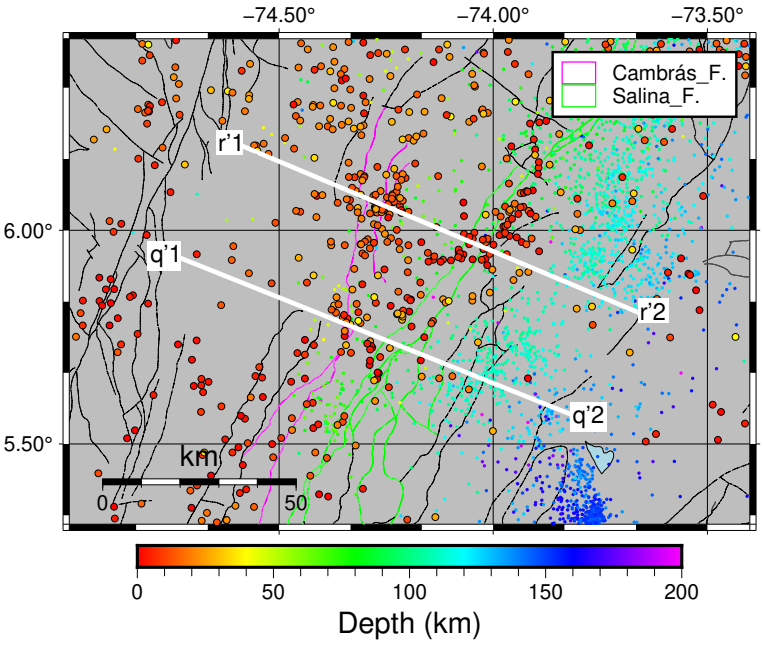

(a) Region of interest.

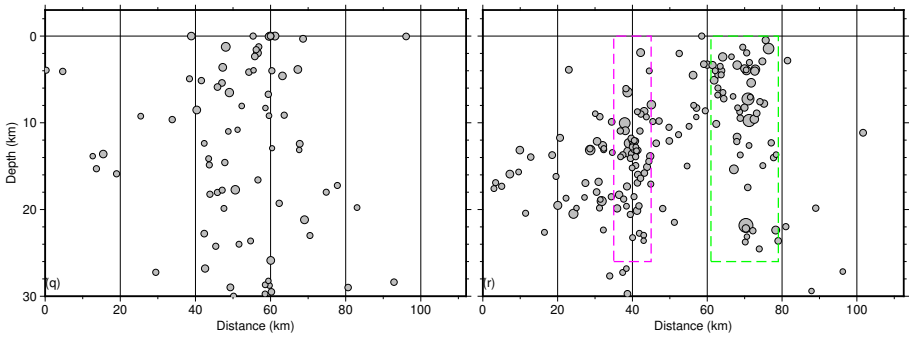

(b) From left to right, q'1-q'2 and r'1-r'2 profiles

Figure 5-9: q'1-q'2 and r'1-r'2 profiles to illuminate the La Salina fault system. They are 12 km wide on each side.

results suggest 17° ± 3 [Hilst and Mann, 1994], and other results measured the flat segment dip at 25° [Malavé and Suárez, 1995, Zarifi et al., 2007] to as much as 40° [van Benthem et al., 2013, Bernal Olaya and Vargas, 2015].

The shallow profile j"1-j"2 (**5-13**) shows lineaments associated with two different system of faults. The first lineament (left side in figure **5-13**-b) is associated to one mining explosion zone. Further southeast, we observe seismicity associated with the Perijá Fault System (figure **5-13**), which are characterized by reverse faults in a NE direction parallel to the foothills [Fuenzalida et al., 1998]. A few kilometers further southwest, at the end of the profile, seismicity associated with the Boconó fault system is delineated. It is one of the fault systems that build the triangular Maracibo block [Fuenzalida et al., 1998]. Last but not least, it is observed that there are several

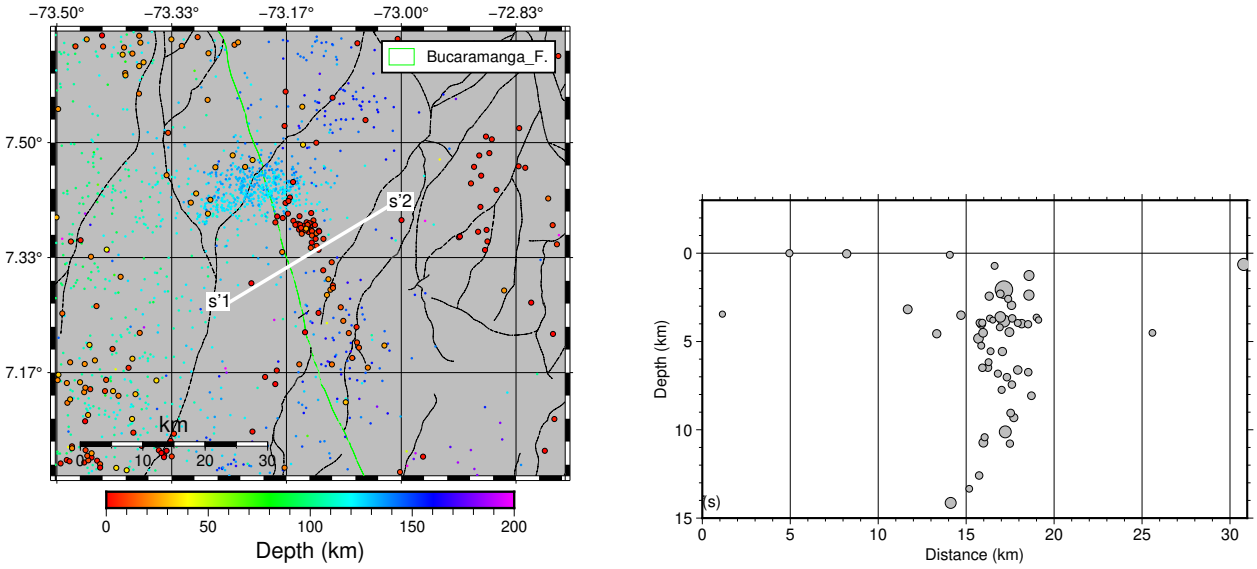

(a) Region of interest

(b) s'1-s'2 profile to illuminate a sector of the Santa Marta Bucaramanga fault.

Figure 5-10: r'1-r'2 profile to illuminate a sector of the Santa Marta-Bucaramanga fault. They are 15 km wide on each side

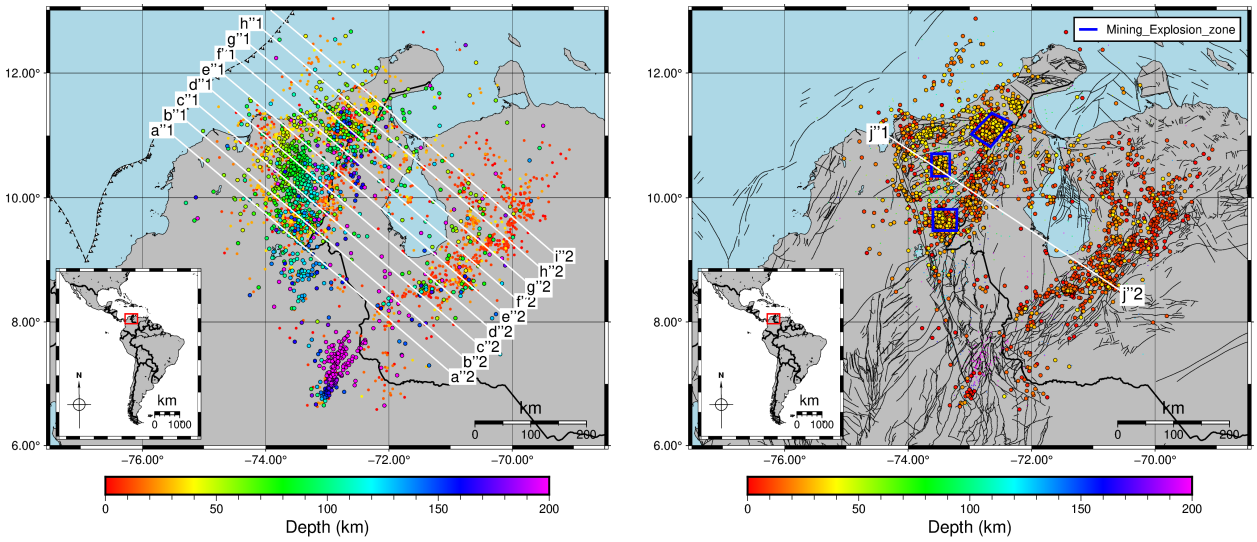

(a) Depths >= 40km are highlighted

(b) Depths <= 40km are highlighted

Figure 5-11: YU catalog.

earthquakes fixed at 9 km depth due to one of the limitations of the HYPOCENTER algorithm.

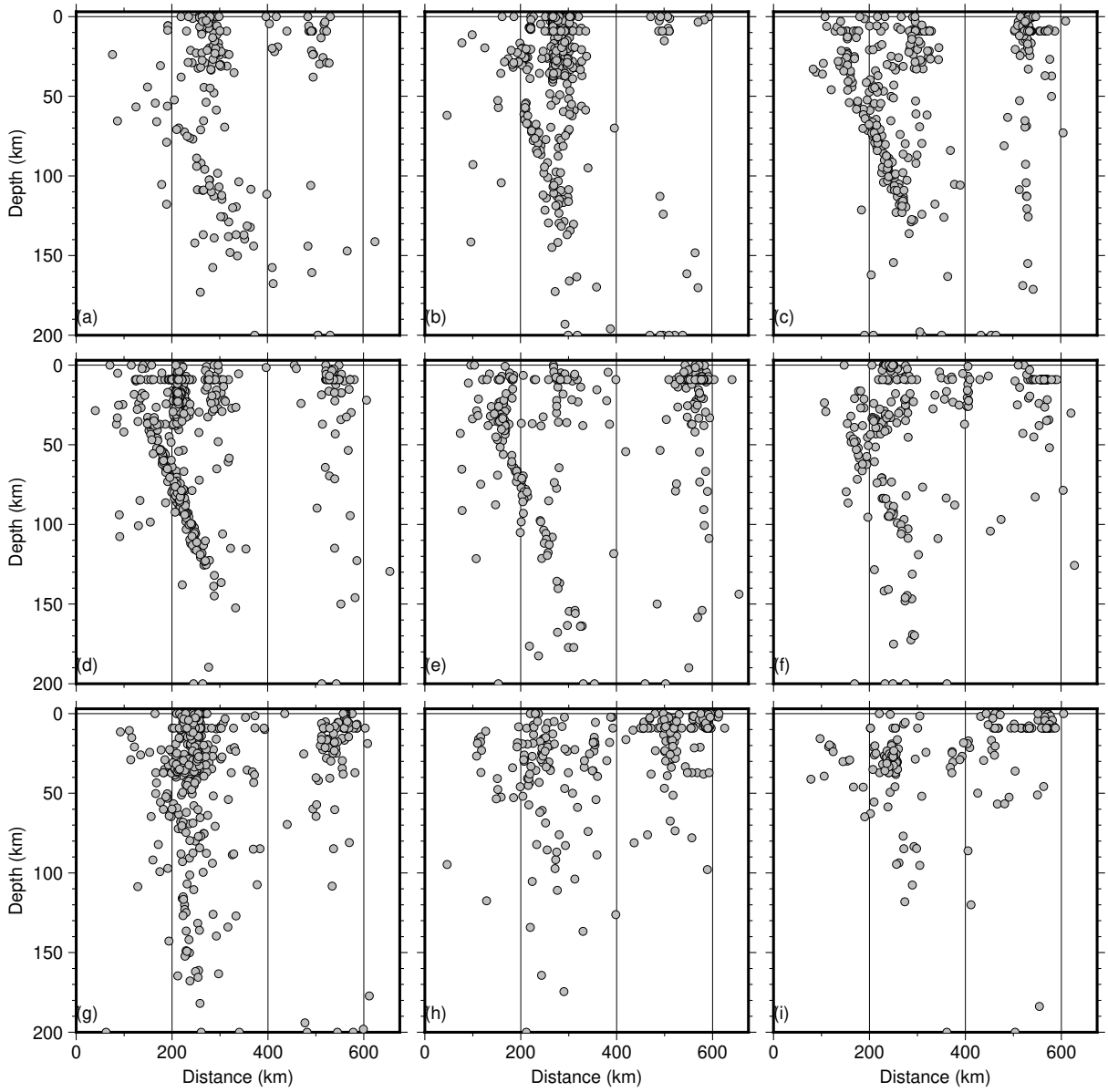

Figure 5-12: a" to i" profiles in the YU network as shown in figure **5-11**-a. They are 17 km wide on each side. So the profiles do not intersect earthquakes between them.

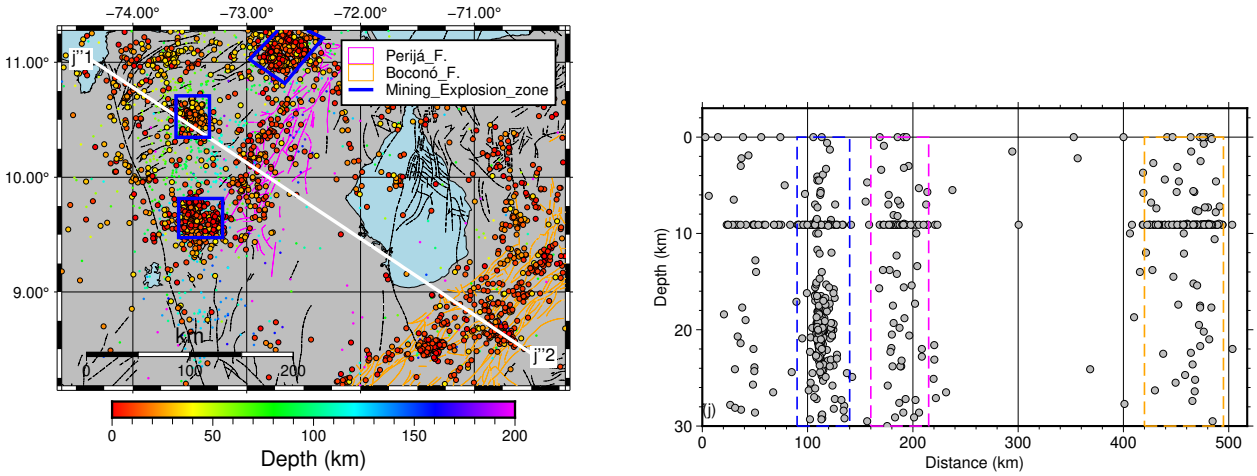

(a) Region of interest.

(b) j"1-j"2 profile to illuminate the Perijá F. and Boconó F.

Figure 5-13: j"1-j"2 profile to illuminate the Perijá F. and Boconó F.. They are 25 km wide on each side.

5.2 Merged automatic catalog

From the above results, we highlight the good performance of EQTransformer as an autopicking algorithm. For the national network, it was able to illuminate the most important faults and structures that the geometry of the stations allowed it to detect. Likewise, it is compatible with the association and location algorithm used in this work. Therefore, we merged the automatic processing of the three networks picked by EQTransformer into a single seismological catalog (figure **5-14**).

Duplicate seismic events were removed giving priority to the network that best located the event. For the local networks we constructed their respective polygons where we expect good locations. Then, events from each local network were only considered if they are inside their respective polygon. Finally, we preferred the VMM network location for duplicate events at the intersection of the polygons.

The catalog illuminates mainly north of 5° because it is the place where most of the processed stations are located. In addition, it is where the VMM network is located, where we processed almost five years of data. The catalog shows each of the annotations we made for each local network. Besides, for both shallow and intermediate depth seismicity, it significantly improves the visualization (figures **5-14**-a and **5-14**-b). For instance, figure **5-14**-b shows the triangular Maracaibo Block bounded by three great strike-dip faults (figure **5-1**-c): *the Boconó Fault (parallel to the Mérida Cordillera) with NE azimuth, the Santa Marta-Bucaramanga Fault trending NNW, and the Oca Fault with EW azimuth* [Fuenzalida et al., 1998].

Finally, for this new catalog, we would like to highlight the strange structure that can be seen near the Bucaramanga nest (Profile A1-A2 in figure **5-15**). In addition, we also want to highlight a

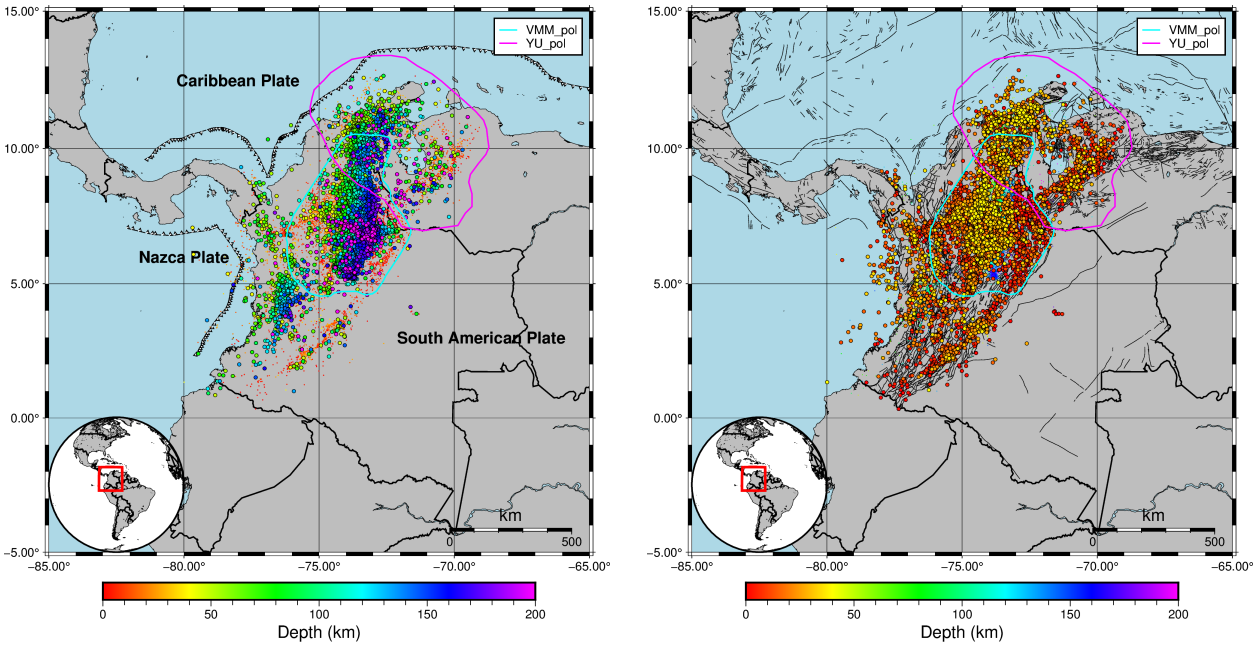

(a) Depths >= 40km are highlighted

(b) Depths < 40km are highlighted

Figure 5-14: Unified automatic catalog

curious intermediate seismicity in the Boconó fault system (Profiles B1-B2 and C1-C2 in the figure **5-15**). Each of these observations should be reviewed in more detail, for example relocating the earthquakes with more sophisticated algorithms, such as Source- Specific Stations Terms method [Richards-Dinger and Shearer, 2000, Martínez and Prieto, 2020], the double difference relocation method [Waldhauser, 2001] or GrowClust [Trugman and Shearer, 2017].

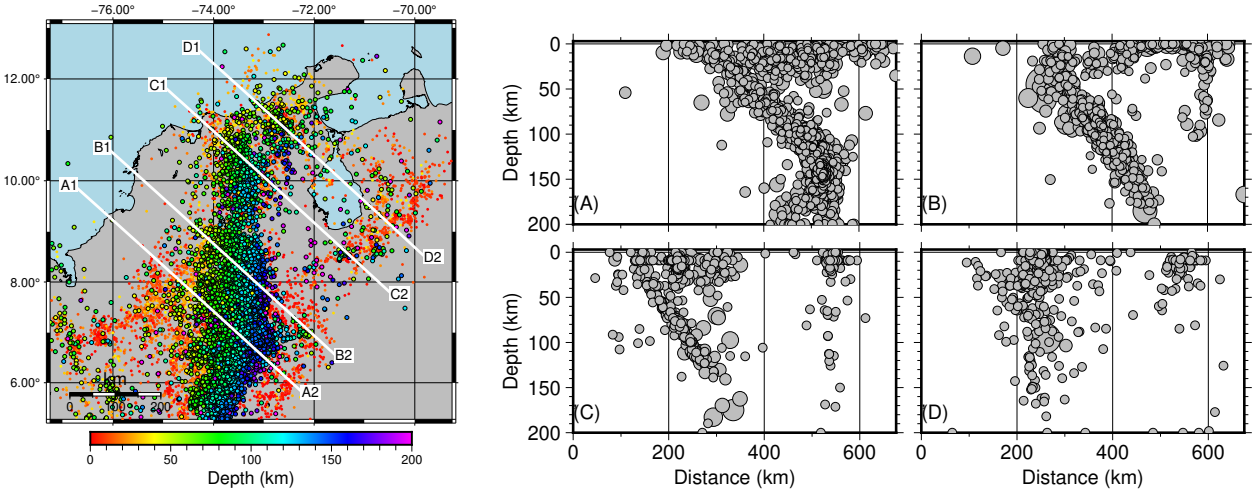

(a) Region of interest

(b) A to D Profiles

Figure 5-15: A to D profiles in the unified automatic catalog. They are 18 km wide on each side.

6 Conclusions

Manual processing of seismological data demands the use of time and personnel. Therefore, there is a need to automate this processing. The most time-consuming task is the detection and autopicking of seismic phases. We presented a detailed analysis of the performance of two pre-trained deep learning models: PhaseNet and EQTransformer. Both are very flexible and operational models, processing large amounts of data in very short times and without requiring sophisticated software or hardware. Besides, they have an incredible ability to pick seismic phases. Their results are comparable to the manual picking, showing better results for small earthquakes or for aftershocks. In terms of detection, PhaseNet shows better abilities to detect small earthquakes, but EQTransformer provides much more confidence in the results. In terms of timing detection quality, both models usually pick the seismic phases at the same time that an analyst would. In terms of the fidelity of the probability value of the picks, EQTransformer probabilities present a better definition of the reality of the pick. The higher the probability of the pick, the more likely it is to correspond to a real phase. The above statement cannot be guaranteed for PhaseNet.

When the picks needed to be associated, most of the PhaseNet picks were rejected because the Scanloc association and location algorithm is quite sensitive to false picks. This is because it works with a relocation methodology. If the solution does not converge, the picks are rejected. So we filtered and re-associated the PhaseNet picks. Our empirical filter allowed us to achieve higher reliability and associate more detections. However, the quantity and quality of the events picked by PhaseNet was severely affected. On the other hand, for EQTransformer, the results did not need any filtering. Nevertheless, only about 30% of the phases were successfully associated for the CM network. In the case of S-phases, Scanloc rejects a large number of true picks due to its relocation methodology.

Comparing their results in terms of reliability and compatibility with the association algorithm, we decided to use only EQTransformer for the two local networks, VMM and YU networks. The same association and location algorithm was used for the VMM network. While, for terms of data privacy in the YU network, we used the free association algorithm proposed in the EQTransformer repository and the Hypocenter locator method. For the VMM network, we observed a great improvement in the percentage of association of the picks due to the fact that it is easier to locate the events. In the case of S-phases, the large number of true picks rejected is better highlighted. When we compare the automatic catalog with the LBG and TECNO manual catalogs, we find that the automatic catalog complements both catalogs for M_w magnitudes greater than 1. Finally, for the YU network, compared to the CM network, the percentage of association was

also improved for both P and S phases.

Both PhaseNet and EQTransformer catalogs are sufficiently reliable to show the same distribution of intermediate and shallow seismicity in the Colombian territory. They are able to show a break or jump in the Benioff zone in the Nazca plate at around $5.5°N$, and also are able to draw the main crustal fault systems, such as The Llanos Foothill Fault System and the Magdalena Valley fault system. Through seismic profiles, we propose that the Bucaramanga nest has an elliptical shape elongating in down-slip direction and is centered at 6.875°N and 73.115°W at a depth of approximately 150 km. At this same location, we observe a sudden change in the strike direction of the Bucaramanga segment. The northern part of the segment has a strike of $\sim N10°E$ until $7°N$. Further south, the segment has a strike $\sim N35°E$.

Local seismic catalogs significantly improve within the area of interest of each respective network. Both complement each other to give a better understanding of the faulting and tectonic setting of northern South America. From the VMM network, we estimated that the northern part of the Bucaramanga segment has a strike of $\sim N5°E$ and the southern has $\sim N28°E$. We also show that there are two seismic clusters in the Colombian territory, the well-documented Bucaramanga nest, and the little studied Cucunubá cluster. Besides, north of $5°N$, the subducted Nazca slab dips at $\sim 50°$, and at most $55°$. Last but not least, at the same epicentral location of the Bucaramanga nest, for depths greater than 150 km, a peculiar curvature not seen in any previous research is shown. The YU network, we observe some interesting crustal lineaments for depths less than 40 km, including mining explosions and the Perijá and Boconó Fault systems. Furthermore, we show the flat subduction of the Caribbean plate beneath northwest South American plate at $\sim 25°$.

Finally, EQTransformer's good performance as an autopicking algorithm and its compatibility with the association and location methods, inspired us to unify the catalogs in only one automatic seismic catalog. It significantly improves the visualization of the seismicity. This catalog was produced in a short time and is the result obtained from an automatic phase picking processing performed by a deep learning model. It is a catalog with an appropriate quality in terms of the event location errors and is capable of defining major tectonic structures. A major drawback of our current processing is the association step. New and improved associators are needed, maybe including ML algorithms. Some recent studies have proposed such new approaches [Ross et al., 2019b, McBrearty et al., 2019a, Zhu et al., 2021], using them could improve automatic catalog performance.

7 Bibliography

[Al-Hashmi et al., 2013] Al-Hashmi, S., Rawlins, A., and Vernon, F. (2013). A wavelet transform method to detect p and s-phases in three component seismic data. *Open Journal of Earthquake Research*, 2:1–20.

[Alan Levander, 2016] Alan Levander (2016). Caribbean-merida andes experiment.

[Allen, 1978] Allen, R. V. (1978). Automatic earthquake recognition and timing from single traces. *Bulletin of the Seismological Society of America*, 68(5):1521–1532.

[Anant and Dowla, 1997] Anant, K. S. and Dowla, F. U. (1997). Wavelet transform methods for phase identification in three-component seismograms. *Bulletin of the Seismological Society of America*, 87(6):1598–1612.

[Baer and Kradolfer, 1987] Baer, M. and Kradolfer, U. (1987). An automatic phase picker for local and teleseismic events. *Bulletin of the Seismological Society of America*, 77(4):1437–1445.

[Bergen and Beroza, 2019] Bergen, K. and Beroza, G. (2019). Earthquake fingerprints: Extracting waveform features for similarity-based earthquake detection. *Pure and Applied Geophysics*, 176.

[Bernal Olaya and Vargas, 2015] Bernal Olaya, R. and Vargas, C. (2015). *Earthquake, Tomographic, Seismic Reflection, and Gravity Evidence for a Shallowly Dipping Subduction Zone beneath the Caribbean Margin of Northwestern Colombia*, pages 247–270.

[Bormann and Saul, 2008] Bormann, P. and Saul, J. (2008). The New IASPEI Standard Broadband Magnitude mB. *Seismological Research Letters*, 79(5):698–705.

[Chiarabba et al., 2016] Chiarabba, C., Gori, P. D., Faccenna, C., Speranza, F., Seccia, D., Dionicio, V., and Prieto, G. A. (2016). Subduction system and flat slab beneath the eastern cordillera of colombia. *Geochemistry*, 17:16 – 27.

[Cichowicz, 1993] Cichowicz, A. (1993). An automatic s-phase picker. *Bulletin of the Seismological Society of America*, 83:180–189.

[Cornthwaite et al., 2021] Cornthwaite, J., Bezada, M. J., Miao, W., Schmitz, M., Prieto, G. A., Dionicio, V., Niu, F., and Levander, A. (2021). Caribbean Slab Segmentation Beneath Northwest South America Revealed by 3-D Finite Frequency Teleseismic P-Wave Tomography. *Geochemistry, Geophysics, Geosystems*, 22(4):1–19.

[Cornthwaite et al., 2017] Cornthwaite, J., Miao, W., Levander, A., Niu, F., Schmitz, M., Dionicio, V., Nader, M., and Bezada, M. (2017). Initial results from the carmarray seismic experiment in northern colombia and western venezuela.

[Cortés et al., 2005] Cortés, M., Angelier, J., and Colletta, B. (2005). Paleostress evolution of the northern andes (eastern cordillera of colombia): Implications on plate kinematics of the south caribbean region. *Tectonics*, 24.

[Dai and MacBeth, 1997] Dai, H. and MacBeth, C. (1997). The application of back-propagation neural network to automatic picking seismic arrivals from single-component recordings. *Journal of Geophysical Research: Solid Earth*, 102(B7):15105–15113.

[Dokht et al., 2019] Dokht, R. M. H., Kao, H., Visser, R., and Smith, B. (2019). Seismic Event and Phase Detection Using Time–Frequency Representation and Convolutional Neural Networks. *Seismological Research Letters*, 90(2A):481–490.

[Earle and Shearer, 1994] Earle, P. S. and Shearer, P. M. (1994). Characterization of global seismograms using an automatic-picking algorithm. *Bulletin of the Seismological Society of America*, 84(2):366–376.

[Fuenzalida et al., 1998] Fuenzalida, H., Dimate, C., and Taboada, A. (1998). Sismotectónica de colombia: deformación continental activa y subducción. *Física de la tierra, ISSN 0214-4557, Nº 10, 1998 (Ejemplar dedicado a: Sismicidad y sismotectónica de Centro y Sudamérica), pags. 111-148.*

[Gentili and Michelini, 2006] Gentili, S. and Michelini, A. (2006). Automatic picking of P and S phases using a neural tree. *Journal of Seismology*, 10(1):39–63.

[Gibbons and Ringdal, 2006] Gibbons, S. J. and Ringdal, F. (2006). The detection of low magnitude seismic events using array-based waveform correlation. *Geophysical Journal International*, 165(1):149–166.

[Hilst and Mann, 1994] Hilst, R. v. d. and Mann, P. (1994). Tectonic implications of tomographic images of subducted lithosphere beneath northwestern South America. *Geology*, 22(5):451–454.

[INGEOMINAS - Servicio Geologico Colombiano (SGC Colombia), 1993] INGEOMINAS - Servicio Geologico Colombiano (SGC Colombia) (1993). Red sismologica nacional de colombia.

[Kellogg et al., 2019] Kellogg, J., Camelio, G., and Mora-Paez, H. (2019). *Cenozoic tectonic evolution of the North Andes with constraints from volcanic ages, seismic reflection, and satellite geodesy*, pages 69–102.

[Kumar et al., 2018] Kumar, S., Vig, R., and Kapur, P. (2018). Development of earthquake event detection technique based on sta/lta algorithm for seismic alert system. *Journal of the Geological Society of India*, 92(6):679–686.

[Lee et al., 2020] Lee, E.-J., Mu, D., Wang, W., and Chen, P. (2020). Weighted template-matching algorithm (wtma) for improved foreshock detection of the 2019 ridgecrest earthquake sequence. *Bulletin of the Seismological Society of America*, 110(4):1832–1844.

[Liu and Zhang, 2014] Liu, H. and Zhang, J.-z. (2014). Sta/lta algorithm analysis and improvement of microseismic signal automatic detection. *Progress in Geophysics*, 29(4):1708–1714.

[Lomax et al., 2000] Lomax, A., Virieux, J., Volant, P., and Berge-Thierry, C. (2000). *Probabilistic Earthquake Location in 3D and Layered Models*, pages 101–134.

[Londoño et al., 2019] Londoño, J. M., Quintero, S., Vallejo, K., Muñoz, F., and Romero, J. (2019). Seismicity of valle medio del magdalena basin, colombia. *Journal of South American Earth Sciences*, 92:565–585.

[Londoño et al., 2020] Londoño, J. M., Vallejo, K., and Quintero, S. (2020). Detailed seismic velocity structure of the caribbean and nazca plates beneath valle medio del magdalena region of ne colombia. *Journal of South American Earth Sciences*, 103:102762.

[Lopez et al., 2020] Lopez, C. M., Velasquez, L., and Dionicio, V. (2020). Calibration of local magnitude scale for colombia. *Bulletin of the Seismological Society of America*, 110:1971–1981.

[Magrini et al., 2020] Magrini, F., Jozinović, D., Cammarano, F., Michelini, A., and Boschi, L. (2020). Local earthquakes detection: A benchmark dataset of 3-component seismograms built on a global scale. *Artificial Intelligence in Geosciences*, 1:1–10.

[Malavé and Suárez, 1995] Malavé, G. and Suárez, G. (1995). Intermediate-depth seismicity in northern colombia and western venezuela and its relationship to caribbean plate subduction. *Tectonics*, 14(3):617–628.

[Marmureanu, 2009] Marmureanu, A. (2009). Rapid magnitude determination for vrancea early warning system. *Romanian Journal of Physics*, 54.

[Martinez, 2016] Martinez, D. (2016). Nazcla plate geometry through seimological data. Undergraduate thesis, Universidad de Caldas, Manizales, Colombia.

[Martínez and Prieto, 2020] Martínez, D. and Prieto, G. A. (2020). Implementación del método de relocalización source specific station terms para colombia: Aplicación para el occidente colombiano. Master's thesis, Universidad Nacional de Colombia, Bogotá, Colombia.

[Mayorga et al., 2020] Mayorga, E., Dionicio, V., Lizarazo, M., Pedraza, P., Poveda, E., Mercado, O., Siervo, D., Aguirre, L., Bolaños, R., Garzón, F., et al. (2020). El sismo de mesetas, meta del 24 de diciembre de 2019 aspectos sismológicos, movimiento fuerte y consideraciones geodésicas. *Bogotá: Servicio Geológico Colombiano*.

[McBrearty, 2021] McBrearty, I., . B. G. C. (2021). Earthquake Phase Association with Graph Neural Networks.

[McBrearty et al., 2019a] McBrearty, I. W., Delorey, A. A., and Johnson, P. A. (2019a). Pairwise Association of Seismic Arrivals with Convolutional Neural Networks. *Seismological Research Letters*, 90(2A):503–509.

[McBrearty et al., 2019b] McBrearty, I. W., Gomberg, J., Delorey, A. A., and Johnson, P. A. (2019b). Earthquake Arrival Association with Backprojection and Graph Theory. *Bulletin of the Seismological Society of America*, 109(6):2510–2531.

[McEvilly and Majer, 1982] McEvilly, T. V. and Majer, E. L. (1982). ASP: An Automated Seismic Processor for microearthquake networks. *Bulletin of the Seismological Society of America*, 72(1):303–325.

[Micallef, 2019] Micallef, T. (2019). Earthquake detection and localisation using the NARS-Botswana data. Master's thesis, Uthrecht University, Utrecht, Netherlands.

[Molina et al., 2020] Molina, I., Velasquez, J., Rubinstein, J., Garcia, A., and Dionicio, V. (2020). Seismicity induced by massive wastewater injection near puerto gaitán, colombia. *Geophysical Journal International*, 223:777–791.

[Mousavi et al., 2020] Mousavi, S. M., Ellsworth, W. L., Zhu, W., Chuang, L. Y., and Beroza, G. C. (2020). Earthquake transformer—an attentive deep-learning model for simultaneous earthquake detection and phase picking. *Nature Communications*, 11(1):1–12.

[Mousavi et al., 2019] Mousavi, S. M., Sheng, Y., Zhu, W., and Beroza, G. C. (2019). Stanford earthquake dataset (stead): A global data set of seismic signals for ai. *IEEE Access*, 7:179464–179476.

[Ojeda and Havskov, 2001] Ojeda, A. and Havskov, J. (2001). Crustal structure and local seismicity in colombia. *Journal of Seismology*, 5:575–593.

[Pardo et al., 2019] Pardo, E., Garfias, C., and Malpica, N. (2019). Seismic phase picking using convolutional networks. *IEEE Transactions on Geoscience and Remote Sensing*, 57(9):7086–7092.

[Pardo Trujillo, 2007] Pardo Trujillo, A., V. C. B. D. M. J. (2007). *Colombian Sedimentary Basins: Nomenclature, Boundaries and Petroleum Geology*. Agencia Nacional De Hidrocarburos-ANH and BM Exploration Ltd. Bogota, Colombia.

[Potsdam, 2018] Potsdam, G. (2018). SeisComP3 documentation.

[Prieto, 2022] Prieto, G. A. (2022). The Multitaper Spectrum Analysis Package in Python. *Seismological Research Letters*, 93(3):1922–1929.

[Prieto et al., 2012] Prieto, G. A., Beroza, G. C., Barrett, S. A., López, G. A., and Florez, M. (2012). Earthquake nests as natural laboratories for the study of intermediate-depth earthquake mechanics. *Tectonophysics*, 570:42–56.

[Richards-Dinger and Shearer, 2000] Richards-Dinger, K. and Shearer, P. (2000). Earthquake locations in southern california obtained using source-specific station terms. *Journal of Geophysical Research*, 105:10939–10960.

[Ringler et al., 2019] Ringler, A., Steim, J., Wilson, D., Widmer-Schnidrig, R., and Anthony, R. (2019). Improvements in seismic resolution and current limitations in the global seismographic network. *Geophysical Journal International*, 220.

[Ronneberger et al., 2015] Ronneberger, O., Fischer, P., and Brox, T. (2015). U-net: Convolutional networks for biomedical image segmentation. *CoRR*, abs/1505.04597.

[Ross et al., 2018a] Ross, Z., Meier, M.-A., and Hauksson, E. (2018a). P wave arrival picking and first-motion polarity determination with deep learning. *Journal of Geophysical Research: Solid Earth*, 123.

[Ross and Ben-Zion, 2014] Ross, Z. E. and Ben-Zion, Y. (2014). Automatic picking of direct P, S seismic phases and fault zone head waves. *Geophysical Journal International*, 199(1):368–381.

[Ross et al., 2018b] Ross, Z. E., Meier, M., Hauksson, E., and Heaton, T. H. (2018b). Generalized Seismic Phase Detection with Deep Learning. *Bulletin of the Seismological Society of America*, 108(5A):2894–2901.

[Ross et al., 2019a] Ross, Z. E., Trugman, D. T., Hauksson, E., and Shearer, P. M. (2019a). Searching for hidden earthquakes in southern california. *Science*, 364(6442):767–771.

[Ross et al., 2019b] Ross, Z. E., Yue, Y., Meier, M.-A., Hauksson, E., and Heaton, T. H. (2019b). Phaselink: A deep learning approach to seismic phase association. *Journal of Geophysical Research: Solid Earth*, 124(1):856–869.

[Sheen and Friberg, 2021] Sheen, D.-H. and Friberg, P. A. (2021). Seismic phase association based on the maximum likelihood method. *Frontiers in Earth Science*, 9.

[Sleeman and van Eck, 1999] Sleeman, R. and van Eck, T. (1999). Robust automatic p-phase picking: an on-line implementation in the analysis of broadband seismogram recordings. *Physics of the Earth and Planetary Interiors*, 113(1):265–275.

[Sun et al., 2022] Sun, M., Bezada, M. J., Cornthwaite, J., Prieto, G. A., Niu, F., and Levander, A. (2022). Overlapping slabs: Untangling subduction in nw south america through finite-frequency teleseismic tomography. *Earth and Planetary Science Letters*, 577:117253.

[Suárez et al., 2008] Suárez, G., Eck, T., Giardini, D., Ahern, T., Butler, R., and Tsuboi, S. (2008). The international federation of digital seismograph networks (fdsn): An integrated system of seismological observatories. *Systems Journal, IEEE*, 2:431 – 438.

[Syracuse et al., 2016] Syracuse, E., Maceira, M., Prieto, G., Zhang, H., and Ammon, C. (2016). Multiple plates subducting beneath colombia, as illuminated by seismicity and velocity from the joint inversion of seismic and gravity data. *Earth and Planetary Science Letters*, 444:139–149.

[Taboada et al., 2000] Taboada, A., Rivera, L., Fuenzalida, H., Cisternas, A., Philip, H., Bijwaard, H., Olaya, J., and Rivera, C. (2000). Geodynamics of the northern andes: Subductions and intracontinental deformation (colombia). *Tectonics*, 19.

[Trnkoczy, 2009] Trnkoczy, A. (2009). Understanding and parameter setting of sta/lta trigger algorithm. In *New Manual of Seismological Observatory Practice (NMSOP)*, pages 1–20. Deutsches GeoForschungsZentrum GFZ.

[Trugman and Shearer, 2017] Trugman, D. T. and Shearer, P. M. (2017). GrowClust: A Hierarchical Clustering Algorithm for Relative Earthquake Relocation, with Application to the Spanish Springs and Sheldon, Nevada, Earthquake Sequences. *Seismological Research Letters*, 88(2A):379–391.

[van Benthem et al., 2013] van Benthem, S., Govers, R., Spakman, W., and Wortel, R. (2013). Tectonic evolution and mantle structure of the caribbean. *Journal of Geophysical Research: Solid Earth*, 118(6):3019–3036.

[Vargas and Mann, 2013] Vargas, C. A. and Mann, P. (2013). Tearing and Breaking Off of Subducted Slabs as the Result of Collision of the Panama Arc□Indenter with Northwestern South America. *Bulletin of the Seismological Society of America*, 103(3):2025–2046.

[Wagner et al., 2017] Wagner, L., Jaramillo, J., Ramirez-Hoyos, L., Monsalve, G., Cardona, A., and Becker, T. (2017). Transient slab flattening beneath colombia. *Geophysical Research Letters*, 44.

[Waldhauser, 2001] Waldhauser, F. (2001). hypodd–a program to compute double-difference hypocenter locations.

[Wang et al., 2019] Wang, J., Xiao, Z., Liu, C., Zhao, D., and Yao, Z. (2019). Deep learning for picking seismic arrival times. *Journal of Geophysical Research: Solid Earth*, 124(7):6612–6624.

[White et al., 2020] White, M., Fang, H., Nakata, N., and Ben-Zion, Y. (2020). Pykonal: A python package for solving the eikonal equation in spherical and cartesian coordinates using the fast marching method. *Seismological Research Letters*, 91.

[Wielandt et al., 2021] Wielandt, E., Caneva, A., and Vargas, C. A. (2021). Desarrollo de los instrumentos de detección y de registro de señales sísmicas. metadatos de las redes sismológicas de la región de latinoamérica y el caribe. *RACCEFYN*, 45(174):313–332.

[Woollam et al., 2019] Woollam, J., Rietbrock, A., Bueno, A., and De Angelis, S. (2019). Convolutional Neural Network for Seismic Phase Classification, Performance Demonstration over a Local Seismic Network. *Seismological Research Letters*, 90(2A):491–502.

[Yarce et al., 2014] Yarce, J., Monsalve, G., Becker, T., Cardona, A., Poveda, E., Alvira, D., and Ordóñez-Carmona, O. (2014). Seismological observations in northwestern south america: Evidence for two subduction segments, contrasting crustal thicknesses and upper mantle flow. *Tectonophysics*, 637.

[Yeck et al., 2019] Yeck, W. L., Patton, J. M., Johnson, C. E., Kragness, D., Benz, H. M., Earle, P. S., Guy, M. R., and Ambruz, N. B. (2019). GLASS3: A standalone multiscale seismic detection associator. *Bulletin of the Seismological Society of America*, 109(4):1469–1478.

[Zarifi et al., 2007] Zarifi, Z., Havskov, J., and Hanyga, A. (2007). An insight into the bucaramanga nest. *Tectonophysics*, 443:93–105.

[Zhu and Beroza, 2019] Zhu, W. and Beroza, G. C. (2019). PhaseNet: A deep-neural-network-based seismic arrival-time picking method. *Geophysical Journal International*, 216(1):261–273.

[Zhu et al., 2021] Zhu, W., McBrearty, I. W., Mousavi, S. M., Ellsworth, W. L., and Beroza, G. C. (2021). Earthquake Phase Association using a Bayesian Gaussian Mixture Model. pages 1–16.